© 2021. Published by The Company of Biologists Ltd | Journal of Cell Science (2021) 134, jcs259306. doi:10.1242/jcs.259306

RESEARCH ARTICLE

The tumor-suppressive long noncoding RNA DRAIC inhibits protein translation and induces autophagy by activating AMPK

Shekhar Saha[1], Ying Zhang[2], Briana Wilson[1], Roger Abounader[2,3] and Anindya Dutta[1,3,4,*]

ABSTRACT

Long noncoding RNAs (lncRNAs) are long RNA transcripts that do not code for proteins and have been shown to play a major role in cellular processes through diverse mechanisms. DRAIC, a lncRNA that is downregulated in castration-resistant advanced prostate cancer, inhibits the NF-κB pathway by inhibiting the IκBα kinase. Decreased DRAIC expression predicted poor patient outcome in gliomas and seven other cancers. We now report that DRAIC suppresses invasion, migration, colony formation and xenograft growth of glioblastoma-derived cell lines. DRAIC activates AMP-activated protein kinase (AMPK) by downregulating the NF-κB target gene GLUT1, and thus represses mTOR, leading to downstream effects, such as a decrease in protein translation and increase in autophagy. DRAIC, therefore, has an effect on multiple signal transduction pathways that are important for oncogenesis, namely, the NF-κB pathway and AMPK–mTOR–S6K/ULK1 pathway. The regulation of NF-κB, protein translation and autophagy by the same lncRNA explains the tumor-suppressive role of DRAIC in different cancers and reinforces the importance of lncRNAs as emerging regulators of signal transduction pathways.

This article has an associated First Person interview with the first author of the paper.

KEY WORDS: DRAIC lncRNA, AMPK, mTORC1, Protein translation, Autophagy

INTRODUCTION

Glioblastoma (GBM) is a highly invasive, migratory and aggressive form of primary malignant tumor in the central nervous system and is responsible for patients morbidity and mortality (Demuth and Berens, 2004; Urbańska et al., 2014; Wen et al., 2020). The highly invasive nature of GBM makes these tumors a major challenge for surgical resection. Despite ionizing radiation and chemotherapy agents like Temozolomide, the average survival of GBM patients is only 12–15 months. Therefore, there is an urgent need to better understand the biology of GBMs in order to develop more effective therapies for patients (Adamson et al., 2009; Anjum et al., 2017; Raizer et al., 2010).

[1]Department of Biochemistry and Molecular Genetics, University of Virginia School of Medicine, Charlottesville, Virginia 22901, USA. [2]Department of Microbiology, Immunology and Cancer Biology, University of Virginia School of Medicine, Charlottesville, Virginia 22901, USA. [3]Cancer Center, University of Virginia, Charlottesville, Virginia 22901, USA. [4]Department of Genetics, University of Alabama, Birmingham, Alabama 35233, USA.

*Author for correspondence (duttaa@uab.edu)

A.D., 0000-0002-4319-0073

Handling Editor: Caroline Hill
Received 19 August 2021; Accepted 28 October 2021

Long noncoding RNAs (lncRNAs) are a class of RNA transcripts that are generally >200 nt in length and do not contain long open reading frames (ORF). Next-generation sequencing discovered a vast number of lncRNAs transcribed from different parts of the genome (Gutschner and Diederichs, 2012; Ransohoff et al., 2018). LncRNAs regulate gene expression both through modulating the epigenetic state and post transcriptionally (Bhan and Mandal, 2014; Hung and Chang, 2010; Statello et al., 2021; Yoon et al., 2013). Abnormal lncRNA expression is often associated with tumor formation, drug resistance and metastasis (Gupta et al., 2010; Malek et al., 2014; Sanchez Calle et al., 2018). It is now well established that lncRNAs can act as tumor promoters (oncogenic) or tumor suppressors and regulate tumor progression and development (Hajjari and Salavaty, 2015; Saha et al., 2020; Sakurai et al., 2015).

We previously reported that DRAIC expression is predictive of favorable outcome in prostate cancers, gliomas and six other cancers (Sakurai et al., 2015), and that the DRAIC lncRNA exerts a tumor-suppressive effect on prostate cancer cells *in vitro* through inhibiting the oncogenic transcription factor NF-κB (Saha et al., 2020). DRAIC interacted with the IκB kinase (IKK) complex, specifically with IKKα and NEMO (encoded by *CHUK* and *IKBKG*, respectively), and disrupted the integrity of the complex, thereby inhibiting IκBα phosphorylation and the downstream NF-κB signaling pathway. DRAIC knockdown or knockout induced NF-κB, cell invasion and soft agar colony formation, and inhibition of NF-κB either by Bay11-7082 or super-repressor IκBα suppressed these phenotypes in prostate cancer (Saha et al., 2020). We have now experimentally tested whether the tumor-suppressive effect of DRAIC can be seen *in vitro* on another cancer, GBM, and elucidated the signal transduction pathway by which this action is mediated.

Mammalian target of rapamycin (mTOR) is a master regulator of cellular protein translation and cell growth (Holz et al., 2005; Wang and Proud, 2006), and is activated by mutations in its regulators in multiple cancers including GBM (Easton and Houghton, 2006). mTOR is a serine-threonine kinase of the phosphoinositide 3-kinase (PI3K) family that is activated by different external stimuli like insulin, amino acids and different growth factors and controls protein translation. mTOR acts via two distinct complexes, mTORC1 and mTORC2. mTORC1 complex consists of five components, of which we want to highlight regulatory-associated protein of mTOR (Raptor; symbol RPTOR). Raptor is often considered an adaptor protein for recruiting mTOR substrates like eukaryotic initiation factor 4E-binding protein 1 (4E-BP1 or EIF4EBP1) and the p70 ribosomal S6 kinase 1 (S6K1; also known as RPS6KB1). mTORC1 stimulates protein translation by phosphorylating 4E-BP1 at threonine (T)37 and T46, which releases EIF4E for it to associate with mRNA caps and thus increases cap-dependent protein translation. mTORC1 also phosphorylates S6K1 at T389, which promotes protein translation.

Journal of Cell Science (2021) 134, jcs259306. doi:10.1242/jcs.259306

mTOR is also known to regulate autophagy, a cellular catabolic process by which cells also maintain energy homeostasis. mTOR inhibits autophagy (Jung et al., 2010; Kim and Guan, 2015) by phosphorylating ULK1 at serine (S)757, which disrupts the interaction between ULK1–AMPK and prevents the activating phosphorylation on ULK1 S555 by AMPK (Egan et al., 2011a). Although inhibiting protein translation usually inhibits tumor progression, the role of autophagy in tumor progression is highly context dependent (Levy et al., 2017; White, 2012). For example, inhibition of autophagy using Bafilomycin A1 and Chloroquine potentiates the effects of chemotherapeutic drugs in triple-negative breast cancer (Chittaranjan et al., 2014), and activation of autophagy is a recognized mechanism of chemo-resistance of GBMs to temozolomide (Jiang et al., 2020; Taylor et al., 2018). On the other hand, autophagy is also responsible for autophagic apoptosis, a known mode of cancer cell killing after chemotherapy and radiotherapy of GBM. Therefore, repression of autophagy may also lead to poor outcome in GBMs (Taylor et al., 2018).

AMP-activated protein kinase (AMPK) is a metabolic energy sensor that maintains cellular energy homeostasis in the presence of energy stress (Gwinn et al., 2008; Hardie and Ashford, 2014). AMPK is a heterotrimeric enzyme that becomes active during energy stress when intracellular concentration of ATP drops and AMP level increases. AMP binds to the γ-regulatory subunit of AMPK, allosterically activates it and accelerates AMPK phosphorylation on T172 by the upstream kinase LKB1 (also known as STK11). Phosphorylation of T172 of AMPK enhances its activity severalfold further (Xiao et al., 2011). AMPK inactivates mTORC1, which leads to the inhibition of protein synthesis and cell growth and an increase in autophagy (Alers et al., 2012; Egan et al., 2011a; Kim et al., 2011). AMPK inhibits mTORC1 by phosphorylating TSC2, an upstream negative regulator of mTORC1 and also by directly phosphorylating Raptor at S792 (Gwinn et al., 2008; Inoki et al., 2003). As mentioned above, AMPK can also phosphorylate ULK1 at S555 residue to induce autophagy (Egan et al., 2011b). In addition, AMPK activation by the adenosine analog 5-aminoimidazole-4-carboxamide riboside (AICAR) leads to an increase in FoxO3a phosphorylation at S413 and upregulation of autophagy regulated genes encoding LC3B-II (the lipidated form of LC3B, encoded by *MAP1LC3B*), Gabarapl1 and Beclin 1 (Mammucari et al., 2007; Sanchez et al., 2012).

Here, we report that DRAIC is also tumor suppressive on GBM cells *in vitro* and that it regulates another signal transduction pathway in GBM and prostate cancer cells. DRAIC exerts its tumor-suppressive function through transmission of the signal from IKK/NF-κB to the AMPK/mTOR pathway via regulation of GLUT1 expression. The inhibition of mTOR by this pathway then leads to inhibition of protein translation and cellular invasion and activation of autophagy.

RESULTS

DRAIC overexpression represses cell migration and invasion in glioblastoma cells

GBM cells often show enhanced cell migration and invasion (Demuth and Berens, 2004; Mair et al., 2018). Prior to determining the effect of DRAIC on GBM cell migration and invasion, we measured DRAIC expression levels in normal immortalized astrocytes, GBM stem cells and GBM cell lines by quantitative real-time RT-PCR (qRT-PCR). Endogenous DRAIC expression levels in these cells are very low compared to those in prostate cancer cells (Fig. S1). We prepared DRAIC overexpressing stable GBM cell lines to examine how DRAIC can be tumor suppressive in these cells. Fig. 1A shows DRAIC overexpression levels in different GBM cell lines. Overexpression of DRAIC in U87 and A172 GBM cells caused decreased cell migration compared to that in cells transfected with empty vector (EV) (Fig. 1B–E). The decreased cell migration caused by DRAIC overexpression in A172 and U87 cells was further validated by time-lapse video microscopy (Movies 1–4). Similar to the decrease in cell migration, DRAIC overexpression in U87, U373 and A172 cells was also associated with reduced cell invasion through Matrigel in a Boyden chamber assay (Fig. 1F–K). These results show that DRAIC overexpression in glioblastoma cells decreases cell migration and invasion.

DRAIC overexpression suppressed tumorigenicity *in vitro* and *in vivo*

Stable overexpression of DRAIC in U87 and U251 cells did not affect cell proliferation when cells were cultured while adherent to a plastic dish (Fig. 2A; Fig. S2) but anchorage independent growth was attenuated, as evident from a decrease in soft agar colony size and colony number as compared to empty vector-expressing cells (EV) (Fig. 2B–E). We next examined the effect of DRAIC on tumor growth *in vivo*. U87 cells stably transfected with either EV or DRAIC-expressing vectors were stereotactically injected into striata of 6-week-old immunodeficient mice and tumor growth was followed by MRI. At 3 weeks after the injection, the EV-expressing U87 group showed large tumors, which are marked in the figure with red arrows, with an average tumor volume of 0.65±0.01 mm^3 (Fig. 2F,H). In contrast, DRAIC-overexpressing U87 cells showed a dramatic reduction of tumor volume to 0.02±0.001 mm^3 (Fig. 2G,H). These results led us to conclude that DRAIC overexpression in GBM cells decreased tumor growth both *in vitro* and *in vivo*.

Note that because of the undetectable levels of DRAIC in GBM cell lines or in GBM-derived stem cells, although overexpression of DRAIC can be studied in GBM and prostate cancer cells, knockdown or knockout experiments below have only been done in prostate cancer cells where DRAIC expression is detected (Saha et al., 2020).

DRAIC regulates global cellular translation

While screening for various oncogenic properties in the cells, we noted that global cellular translation, as measured by puromycin pulse labeling is regulated by DRAIC. Overexpression of DRAIC in both GBM and prostate cancer cells led to decreased global cellular translation (Fig. 3A,B). Conversely, knockdown or knockout (KO) of DRAIC in prostate cancer cells stimulated protein translation (Fig. 3C,D). Since high mTORC1 activity in tumor cells is often associated with increased cellular translation (Guertin and Sabatini, 2007; Pópulo et al., 2012), we examined whether mTORC1 is activated when DRAIC is knocked down or knocked out. The phosphorylation of mTORC1 at S2448 is sometimes considered a surrogate marker for mTOR activation (Chiang and Abraham, 2005). DRAIC overexpression did not reduce mTOR phosphorylation at this residue (Fig. 3E) but decreased the phosphorylation of the mTOR substrate S6K1 (T389) (Fig. 3E). Knockout of DRAIC in prostate cancer cells again did not affect the mTOR phosphorylation at S2448 residue but increased the phosphorylation of S6K1 and of the S6K substrate S6 (Fig. 3F). Consistent with regulation of mTORC1, the phosphorylation of another mTORC1 substrate, ULK1 on S757, was decreased by overexpression of DRAIC and increased by knockout of DRAIC (Fig. 3G,H). These results suggest that DRAIC regulates cellular phenotypes, including global protein translation, by modulating the activity of mTOR kinase.

Journal of Cell Science (2021) 134, jcs259306. doi:10.1242/jcs.259306

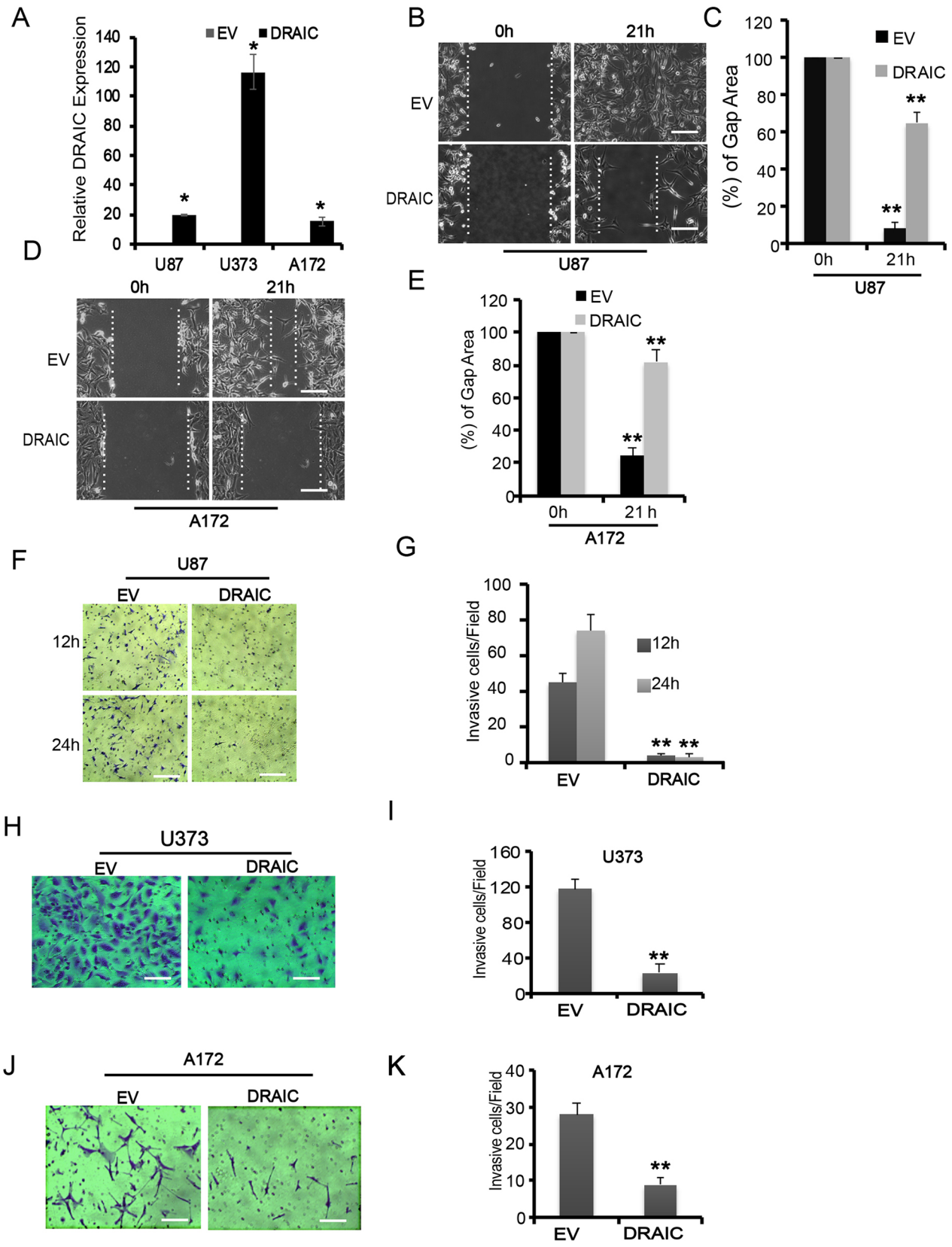

Fig. 1. DRAIC suppresses glioblastoma cell migration and invasion. (A–E) A172 U87 and U373 GBM cells were stably transfected with either empty vector or full-length DRAIC, and the DRAIC overexpression was quantified by qRT-PCR (A). The monolayer cells from U87 (B) and A172 (D) cells were scratched using 200 µl filter tips and allowed the cells to migrate over 21 h. The images were captured at 0 and 21 h time point. The scratch width or gap area (dotted lines) was calculated using ImageJ software and quantified in C and E. (F–K) Matrigel invasion assay was performed with DRAIC overexpressing U87 (F,G), U373 (H,I) and A172 (J,K) cells. The average number of invasive cells were quantified by counting cells from 10 random fields for each cell line. Scale bars: 20 µm. Data are presented as mean±s.d. from three independent experiments. *P<0.05, **P<0.01 (two-tailed Student's t-test).

Journal of Cell Science (2021) 134, jcs259306. doi:10.1242/jcs.259306

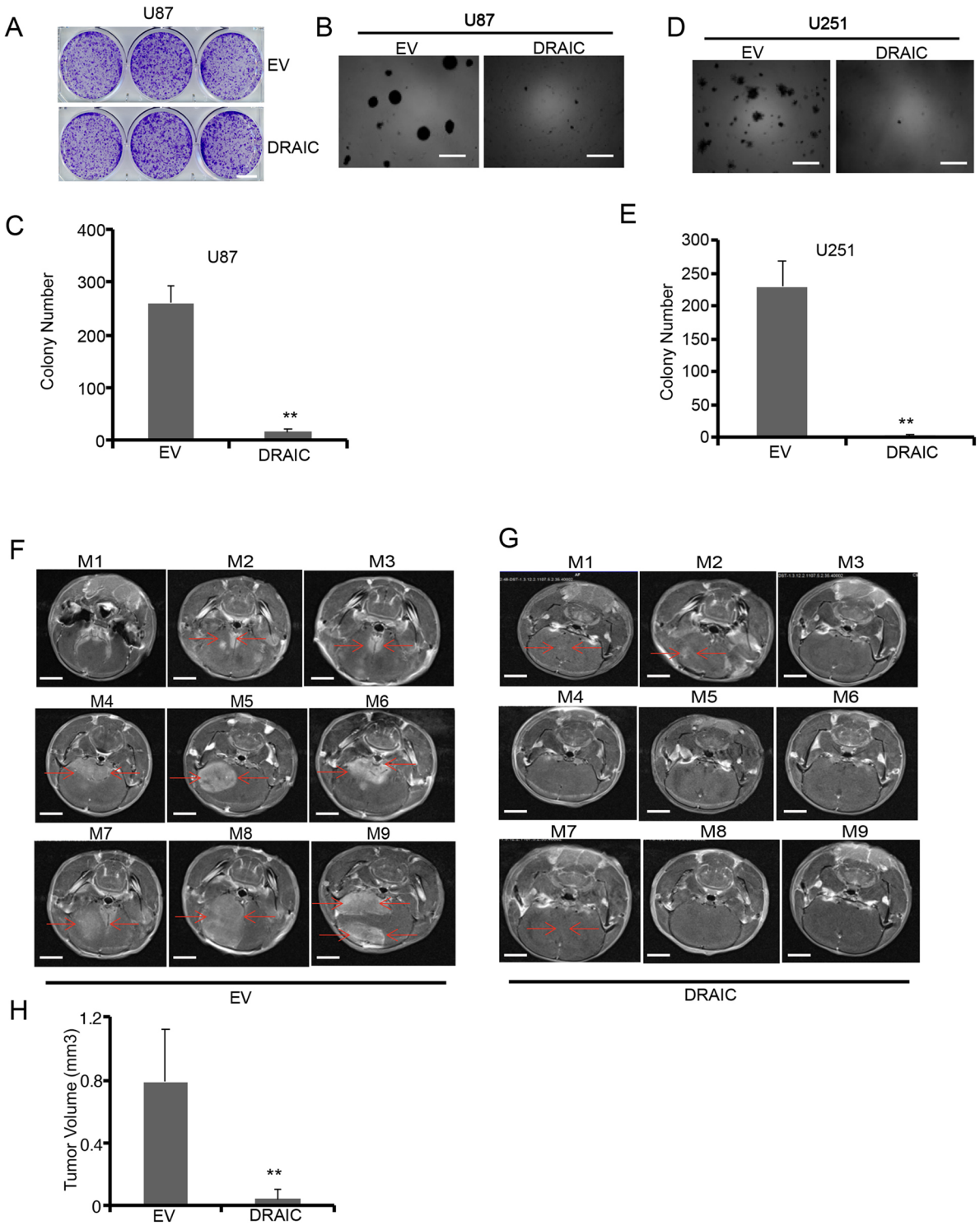

Fig. 2. DRAIC overexpression represses the tumorigenic property of glioblastoma cells both *in vitro* and *in vivo*. (A) A colony formation assay was carried out with EV- and DRAIC-overexpressing U87 cells. Scale bars: 5 mm. (B–E) Anchorage-independent soft agar colony formation was executed in U87 (B,C) and U251 cells (D,E). 10^4 cells were seeded for the soft agar assay and monitor the growth of the cells over 3 weeks (B,D). The colony number was quantified by taking an average of 10 random field (C,E). Scale bars: 50 µm. (F,G) 2×10^5 U87 cells either transfected with EV (n=9) (F) or full-length DRAIC (n=9) (G) were stereotactically implanted into the stratia of immunodeficient mice brain. 3 weeks after the injection, the mice were imaged by MRI scan and data is quantified in G. Arrows highlight the location of the tumor. Data are presented as mean±s.d. from three independent experiments. Scale bars: 0.5 mm. *P<0.05, **P<0.01 (two-tailed Student's t-test).

DRAIC regulates AMPK and thus regulates mTORC1

The mTOR pathway is regulated indirectly by several upstream kinases (Sarbassov et al., 2005), particularly by AMPK (Shaw, 2009; Xu et al., 2012). The schematic in Fig. 4A shows the different substrates that are phosphorylated and regulated by AMPK. To understand the mechanism of decreased mTOR substrate phosphorylation upon DRAIC overexpression, we checked the AMPK phosphorylation status at the T172 residue, a marker for

Journal of Cell Science (2021) 134, jcs259306. doi:10.1242/jcs.259306

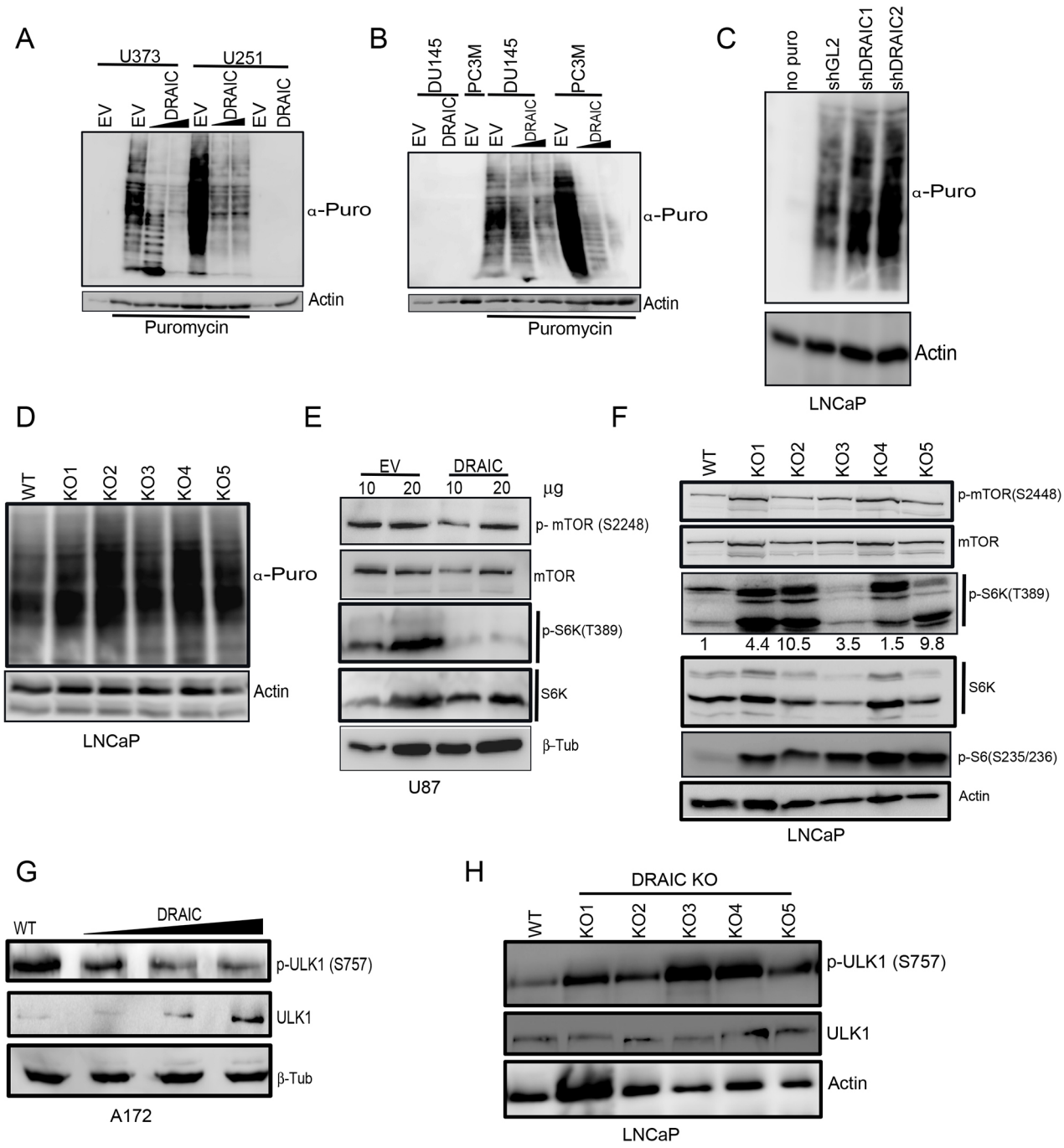

Fig. 3. Low DRAIC expression is associated with increased cellular translation in glioblastoma. (A,B) U373, U251 (A), DU145 and PC3M cells (B) were transfected with either EV or DRAIC followed by 10 µg/ml puromycin pulse labeling for 1 h and immunoblotted with antibodies against puromycin and loading control actin. (C,D) LNCaP cells with either stable DRAIC knockdown (C) or knockout (D) of DRAIC were pulse labeled with puromycin for 1 h and cell lysates were subjected to immunoblotting with the antibodies against puromycin and actin. (E) U87 cells were transfected with either EV or full-length DRAIC and 10 and 20 µg of cell lysates was loaded and immunoblotted with antibodies against phospho-mTORC1 (S2448), phospho S6K (T389), total S6K and α-tubulin. (F) EV and DRAIC KO LNCaP cell lysates were immunoblotted with antibodies against phospho mTORC1 (S2448), phospho-S6K (T389), total S6K, phospho-S6 (S222/S223) and loading control actin. A quantification of p-S6K signal normalized to S6K signal for the blot shown is presented. (G) A172 cells were stably transfected with EV and DRAIC overexpressing plasmids and cell lysates were immunoblotted with antibodies against phospho-ULK1 S757, ULK1 and tubulin. (H) Different KO single clones of DRAIC were immunoblotted with antibodies against phospho ULK1, ULK1 and actin. Data are representative of three independent experiments.

AMPK kinase activity. Overexpression of DRAIC in A172 GBM cells increased AMPK phosphorylation (Fig. 4B) whereas DRAIC KO in the prostate cancer cell line (LNCaP cells) decreased AMPK phosphorylation (Fig. 4C). One of the mechanisms by which AMPK inhibits mTOR activity is by phosphorylating Raptor at S792 (Gwinn et al., 2008). Overexpression of DRAIC in A172 and U251 cells increased Raptor phosphorylation on S792 (Fig. 4D,E), whereas DRAIC KO decreased Raptor phosphorylation on S792 (Fig. 4F). Two other substrates of AMPK, ULK1 (S555) and FoxO3A (S413), were phosphorylated upon DRAIC overexpression suggesting that AMPK activity is globally induced upon DRAIC overexpression (Fig. 4G–K), whereas DRAIC KO decreased the level of phosphor-

Journal of Cell Science (2021) 134, jcs259306. doi:10.1242/jcs.259306

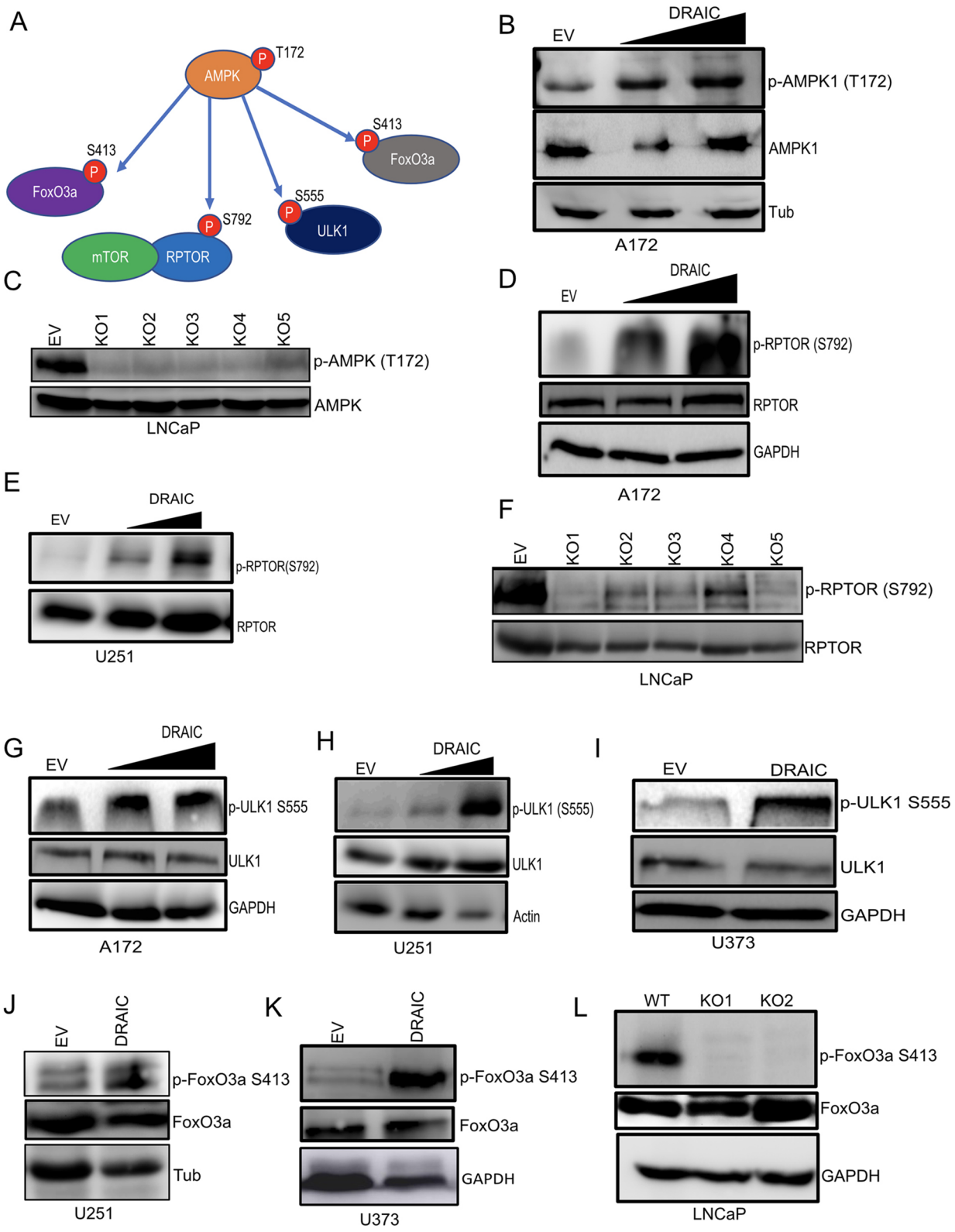

Fig. 4. DRAIC regulates AMPK substrate phosphorylation. (A) Schematic representation of different substrates that are phosphorylated by AMPK. (B) Empty vector (EV) and DRAIC-overexpressing A172 cells were immunoblotted with antibodies against phospho-AMPK (T172), total AMPK and loading control tubulin. (C) WT and multiple DRAIC KO clones were subjected to immunoblotting with antibodies against phospho-AMPK (T172) and total AMPK. (D–F) EV and DRAIC-overexpressing cells from A172 (D) and U251(E) or DRAIC KO (F) clones from LNCaP cells were subjected to immunoblotting with antibodies against phospho-Raptor S792 and total Raptor. (G–I) EV and stable DRAIC-overexpressing cells from A172 (G), U251 (H) and U373 (I) cells were subjected to immunoblotting with antibodies against phospho-ULK1 (S555), total ULK1 and loading control GAPDH. (J–L) EV and DRAIC-overexpressing cells from U251(J) and U373(K) or DRAIC KO LNCaP (L) cells were subjected to western blotting with antibody against phospho-FoxO3a (S413). Data are representative of two independent biological experiments.

Journal of Cell Science (2021) 134, jcs259306. doi:10.1242/jcs.259306

FoxO3A S413 (Fig. 4L). Together these results suggest that DRAIC stimulates AMPK, and this inhibits mTORC1 to inhibit phosphorylation of key substrates like S6K1, which inhibits translation.

DRAIC overexpression induces autophagy and associated gene expression

AMPK regulates cellular energy metabolism and homeostasis by controlling autophagy (Alers et al., 2012; Kim et al., 2011). Indeed, the increase in ULK1 S555 and FoxO3A S413 phosphorylation upon DRAIC overexpression (Fig. 4) would be expected to promote autophagy. DRAIC overexpression in U251 cells decreased the levels of LC3B-II and p62 (also known as SQSTM1) (Fig. 5A), the core proteins involved in autophagosome formation, which are subsequently degraded when the autophagosomes fuse to lysosomes (Nakamura and Yoshimori, 2017). To distinguish whether the decrease of LC3B-II level is due to the inhibition of autophagosome formation or increased lysosomal degradation, DRAIC overexpressing cells were treated with bafilomycin A1 to inhibit lysosomal degradation. Bafilomycin A1 restored the level of

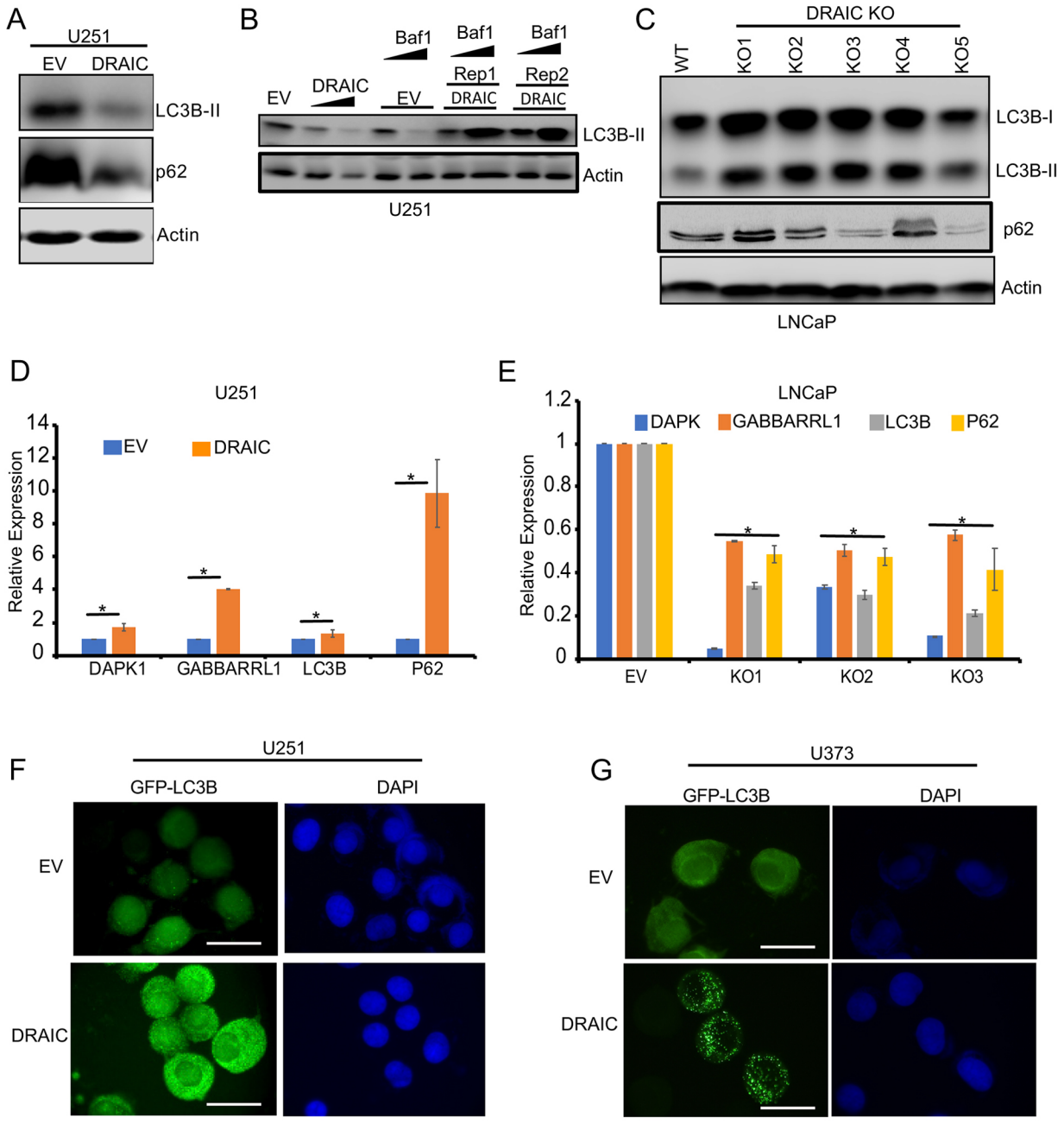

Fig. 5. Overexpression of DRAIC induces autophagy. (A) U251 cells transfected with EV and DRAIC were immunoblotted with antibodies against LC3B, p62 and internal loading control actin. (B) U251 cells were stably transfected with empty vector (EV) or full length DRAIC were treated with 10 nM of bafilomycin A1 for 24 h and cell lysates were subjected to immunoblotting with LC3B and actin antibodies. (C) WT and DRAIC KO LNCaP clones were immunoblotted with antibodies against LC3B, p62 and actin. (D,E) qRT-PCR analysis of autophagy responsive gene expression in U251 cells (D) and DRAIC KO LNCaP cells (E). (F,G) DRAIC overexpressing U251 (F) and U373 (G) cells were transfected with GFP tag LC3B and puncta formation was assessed to monitor the autophagosome formation. Scale bars: 10 µm. Data are presented as mean±s.d. from three independent experiments. *P<0.05 (two-tailed Student's t-test).

Journal of Cell Science (2021) 134, jcs259306. doi:10.1242/jcs.259306

LC3B-II in DRAIC overexpressing cells, suggesting that lysosomal degradation of LC3B-II and, by extension, autophagic flux, is increased when DRAIC is elevated in GBM cells (Fig. 5B, compare lane 1 with 2 and 3). Knockout of DRAIC in LNCaP cells increased LC3B-II expression suggesting the inhibition of autophagy (and inhibition of lysosomal degradation) of LC3B-II. Consistent with a decrease in DRAIC being associated with a decrease in autophagic flux, and despite a decrease in p62 mRNA, the level of p62 protein (normally degraded by autophagolysosomes, whose formation is inhibited) is increased in three of the DRAIC KO prostate cancer cells [Fig. 5C, KO1, KO2, KO4 compared to wild type (WT)] and unchanged in the other two. The DRAIC-AMPK pathway increased the phosphorylation and activation of FoxO3A, a transcription factor important for induction of genes associated with autophagy (Fig. 4J,K). Consistent with this, DRAIC overexpression increased the expression of autophagy-associated genes, whereas DRAIC KO decreased expression of those same genes (Fig. 5D,E,).

Finally, we performed microscopic imaging of LC3B by fusing it with a GFP tag to express a chimeric GFP–LC3B that can mark autophagosome formation as fluorescent puncta (Cohen-Kaplan et al., 2016). DRAIC overexpression in both U251 and U373 cells increased GFP–LC3B puncta consistent with an induction of autophagy (Fig. 5F,G).

Overall, these results suggest that DRAIC overexpression leads to an increase in autophagy while decreasing protein translation, and conversely a decrease in DRAIC, as in the DRAIC KO cells, decreases autophagy along with an increase in translation. Thus, DRAIC elevation mimics conditions of energy stress or amino acid starvation, and this might be responsible for the suppression of oncogenic phenotypes.

DRAIC KO-induced protein translation and cellular invasion are reversed by activating AMPK

To understand whether increased protein translation seen upon DRAIC KO LNCaP is mediated by a decrease in active AMPK, we pre-treated both WT and DRAIC KO LNCaP cells with the AMPK activators AICAR or metformin for 24 h and performed a global protein translation assay with puromycin pulse labeling. Both AMPK activators rescued the DRAIC KO-mediated increase in global protein translation (Fig. 6A). The WT and DRAIC KO LNCaP cells were also treated with different concentrations of rapamycin, a well-known inhibitor of mTORC1 and cellular translation, as a positive control in our experiment (Fig. 6A).

We also checked whether the increased cellular invasion seen upon DRAIC KO is because of AMPK inhibition, by inducing AMPK activity with AICAR treatment or by overexpressing constitutive active AMPK, and then performing the Matrigel Boyden chamber invasion assay. Both the chemical and genetic activation of AMPK led to a decrease in cell invasion in DRAIC KO LNCaP cells (Fig. 6B, C; Fig. S3). Here again, rapamycin treatment demonstrates that the increase in protein translation (downstream of AMPK inhibition) also decreases the cellular invasion in DRAIC KO LNCaP cells.

Taken together, these results suggest that AMPK inhibition in DRAIC-deficient cells is responsible for the increase in cellular translation and increase in invasion (Fig. 6B,C; Fig. S3). The effects of rapamycin on protein translation and invasion suggest that the increased invasion is dependent on the increase in protein translation.

The interplay of IKK–NF-κB with AMPK–mTOR–protein translation and cell invasion

DRAIC KO, by inhibiting IKK, activates the NF-κB pathway (Saha et al., 2020). We previously showed that DRAIC KO-induced invasion could be rescued by inhibiting IKK and NF-κB. Above, we showed that the increase in invasion and protein translation can also be rescued by activating AMPK. This raises the question of whether IKK and the NF-κB pathway is involved in transmitting the signal from DRAIC through AMPK to protein translation and cellular invasion. To understand the involvement of DRAIC in attenuating cellular translation through the NF-κB pathway, we inhibited NF-κB in DRAIC KO cells by four strategies – transfecting plasmids overexpressing IκBα super repressor (S32A/S36A) (1) or the catalytically dead IKKβ kinase (IKK2-dominant negative) (2), or knocking down NF-κB p65 (also known as RelA) by siRNA (3) or treatment with the IKK inhibitor Bay11-7082 (4). Inhibition of NF-κB pathway by any of the above strategies reversed the increase in protein translation in DRAIC KO cells (Fig. 6D–F).

Increase in cellular invasion and translation in DRAIC KO LNCaP cells is reversed by inhibiting NF-kB target gene GLUT1

We next asked how NF-κB activity (seen upon DRAIC KO) could suppress AMPK activity. Increase in NF-κB target gene expression is often associated with increased tumorigenicity and metastasis (Xia et al., 2014). NF-κB and IKK are known to increase the expression and surface localization of the NF-κB target gene GLUT1 (Wang et al., 2019), which would result in increased glucose import and so a decrease in the AMP:ATP ratio in cells, which may be sufficient to decrease AMPK activation. To explore the involvement of GLUT1 in regulating AMPK activity, we assessed the expression of GLUT1 in DRAIC KO and overexpressing cells. GLUT1 mRNA and protein expression is increased in DRAIC KO cells and deceased in DRAIC overexpressing cells (Fig. 7A,B; Fig. S4). The increase in cellular invasion and translation seen in DRAIC KO cells can also be reversed by inhibiting GLUT1 with the pharmacological inhibitor Bay-876 (Fig. 7C–E). We conclude that increased GLUT1 expression is responsible for induction of cellular invasion and induction of protein translation in DRAIC KO cells.

As DRAIC KO decreased AMPK phosphorylation at T172, we asked whether this effect is due to the increase in GLUT1 expression, which is known to regulate the activity of AMPK by regulating the ratio of AMP/ATP. An increased AMP/ATP ratio leads to allosteric activation of AMPK through the binding of AMP to the γ-subunit of AMPK. To assess whether the elevation of GLUT1 is responsible for the inhibition of AMPK activity we followed AMPK activity by immunoblotting for another AMPK target, phospho (p)-ACC S79 (phospho-acetyl-CoA carboxylase, encoded by *ACACA*). DRAIC KO cells show decreased p-ACC S79 expression, consistent with the low activation of AMPK. However, treatment of the DRAIC KO cells with GLUT1 inhibitor rescued the ACC phosphorylation, suggesting that the inhibition of AMPK was indeed mediated by the increase of GLUT1 (Fig. 7F). To add to the evidence, we measured the cellular AMP level in DRAIC KO cells and discovered that the AMP concentration is decreased in DRAIC KO cells, and that this reduction in AMP is rescued by inhibiting the NF-κB pathway either with the IKK inhibitor Bay11-7082 or by knocking down p65 (Fig. 7G). In contrast, overexpression of DRAIC in U373 cells, which decreases GLUT1 expression (Fig. S4), leads to an increase of AMP level (Fig. 7H). These results suggest that increased GLUT1 expression in DRAIC KO cells leads to reduction of AMP/ATP ratio, which decreases AMPK activity and thus increases cellular translation.

Journal of Cell Science (2021) 134, jcs259306. doi:10.1242/jcs.259306

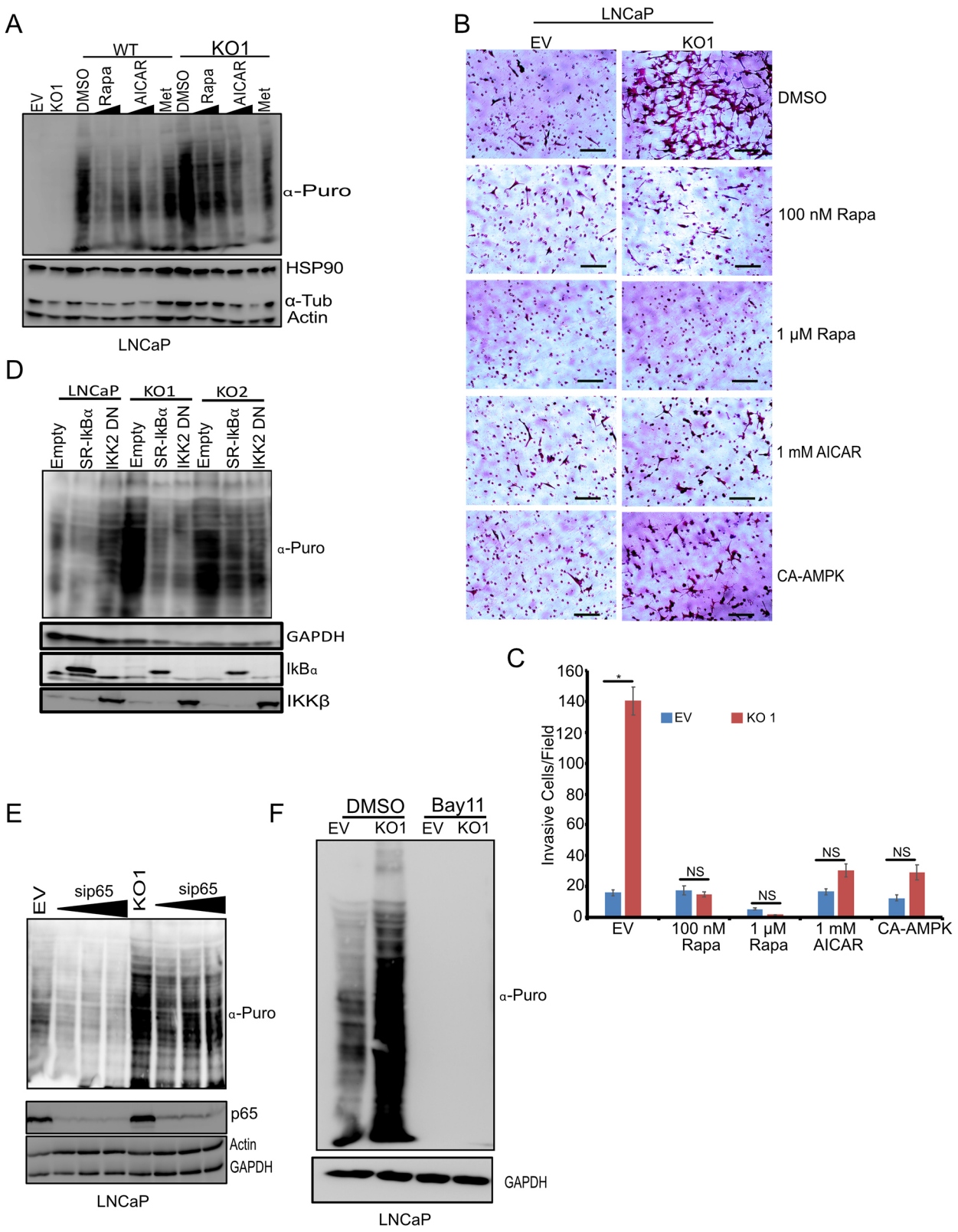

Fig. 6. See next page for legend.

DISCUSSION

Our results identify a major signal transduction pathway through which DRAIC mediates its tumor-suppressive effect on cancer cells of different lineages. As in prostate cancer, DRAIC suppresses glioblastoma development both *in vitro* and *in vivo*. We discovered the following. First, that overexpression of DRAIC in different glioblastoma cells decreased cell migration, cell invasion, anchorage-independent growth and xenograft growth. Second, that DRAIC decreases protein translation through inhibiting the phosphorylation of mTORC1 substrates. Third, that DRAIC induces AMPK

Journal of Cell Science (2021) 134, jcs259306. doi:10.1242/jcs.259306

Fig. 6. DRAIC KO induced translation and invasion were rescued by AMPK activators. (A) LNCaP and DRAIC KO cells were pre-treated either with translation inhibitor, rapamycin or 1 mM of the AMPK activators AICAR and metformin for 24 h followed by puromycin pulse labeling and immunoblotting with puromycin antibody. (B,C) WT and DRAIC KO LNCaP cells transfected with constitutive active AMPK or pre-treated with 0.1, 1 µM rapamycin or AMPK activator AICAR for 24 h and Boyden chamber invasion assay was performed. 10 random fields were selected for counting the number of invasive cells per field. (D) LNCaP and DRAIC KO cells were transfected with either super repressor IκBα (SR-IκBα) or IKKβ dead kinase mutant (IKK2-DN) for 48 h followed by puromycin pulse labeling and immunoblotting with puromycin antibody. (E,F) LNCaP and DRAIC KO cells were transfected with siRNA against p65 or treated with IKK inhibitor Bay11-7082 for 2 h followed by puromycin pulse labeling and immunoblotting with antibodies against puromycin, p65, actin and GAPDH. Scale bars: 20 µm. Data are presented as mean±s.d. from three independent experiments. **P*<0.05 (two-tailed Student's *t*-test).

phosphorylation at T172 residue, which is known to repress mTORC1 to repress translation and phosphorylates several substrates that lead to an increase in autophagic flux. And finally, that the increase in translation after DRAIC knockout is reversed by inhibiting IKK kinase activity, knocking down p65 or activating AMPK. Taken together these results support a model (Fig. 8) where DRAIC inhibits several tumor phenotypes in prostate cancers and gliomas by inhibiting NF-κB, and thus activating AMPK, inhibiting mTORC1, inhibiting protein translation and increasing autophagy. The link between NF-κB and AMPK is mostly mediated by the ability of NF-κB to induce the glucose transporter GLUT1. Thus, when DRAIC is decreased in tumors, NF-κB is activated, leading to increased glucose uptake and decreased AMP/ATP ratio and repression of AMPK. This results in increase of protein translation through mTORC1 activation and inhibition of autophagy through AMPK repression. So, at least in this context, inhibition of autophagy appears to make tumors more aggressive, consistent with the notion that autophagic apoptosis is important for GBM cell death following temozolamide and radiotherapy.

It is interesting that, although previous literature has reported that mTOR and Raptor both are associated with the IKK complex (Dan et al., 2008), our results with AICAR and metformin (activators of AMPK) suggest that the effect of IKK on mTORC1 is mediated through AMPK.

Our results add DRAIC to the list of a few lncRNAs that are known to be involved in regulating the mTORC1 pathway. The H19 lncRNA controls pituitary tumor growth by inhibiting the mTORC1 pathway. H19 interacts with the TOS domain of 4E-BP1 and masks the Raptor-binding site and therefore inhibits the 4E-BP1 phosphorylation by mTORC1 without affecting S6K1 phosphorylation (Wu et al., 2018). The lncRNA MALAT1 is oncogenic in hepatocellular carcinomas, and acts by inducing the expression of the oncogenic splicing factor SRSF1, which promotes the expression of a short isoform of S6K1 that binds with mTORC1 and activates the kinase (Malakar et al., 2017). HAGLROS directly binds to and activates mTOR and acts as a competing endogenous RNA to antagonize miR-100-5p and thus increases mTOR expression (Chen et al., 2018). DLEU1 has been shown to associate with mTOR, although it is not clear whether the binding regulates mTORC1 (Du et al., 2018). In contrast to the other lncRNAs, however, DRAIC does not physically associate with mTOR (data not shown) and appears to act on mTOR by regulating its upstream activator AMPK.

Recent literature suggests that there are a few lncRNAs that modulate AMPK activity. The lncRNA NBR2 interacts with AMPK during energy deprivation to activate AMPK, and its expression is induced by LKB1-AMPK thereby producing a feed-forward loop to activate AMPK (Li et al., 2016). Depletion of the oncogenic lncTHOR inhibits glioma cell survival by decreasing MAGEA6 mRNA and protein, which leads to decreased degradation of AMPKα by MAGEA6-TRIM28 E3 ubiquitin ligase (Xue et al., 2019). The increase of AMPK level and activity is detrimental to glioma cell survival. We now report that DRAIC also promotes AMPK activation and suppresses tumor progression. However, here again, we did not see any direct association of DRAIC with AMPK or with any of the activating kinases of AMPK.

We show that DRAIC regulates the AMPK pathway through NF-κB. DRAIC reduces the expression of the glucose transporter GLUT1, an NF-κB-responsive gene, which leads to decreased uptake of glucose through GLUT1 and an increase in the ratio of AMP/ATP. This increased intracellular concentration of AMP leads to activation of AMPK pathway and stimulation of autophagy in cells overexpressing DRAIC.

A consistent tumor-suppressive role of DRAIC *in vitro* on prostate cancer and glioblastoma suggests that this is an effect generalizable to multiple lineages. This is consistent with the finding that decreased DRAIC expression predicts poor outcome in eight different malignant tumors (Sakurai et al., 2015). However, there are a few studies on DRAIC specifically in breast cancer that show it might act as an oncogenic lncRNA by regulating different cellular functions, but the molecular mechanism behind this oncogenic nature is not clearly understood (Sun et al., 2015; Tiessen et al., 2019; Zhao and Dong, 2018). DRAIC knockdown in MCF7 breast cancer cells increases autophagic flux (Tiessen et al., 2019). In contrast, we note that in both GBM and prostate cancer cells DRAIC overexpression increases autophagic flux and DRAIC knockout increases p62 levels, consistent with a decrease in autophagic flux (Fig. 5). The opposite effects that DRAIC appears to have on tumor progression in these lineages (oncogenic in breast, tumor suppressive in prostate and gliomas) could be explained by the lineage-specific opposite effects of DRAIC on autophagic flux. Despite these tissue-specific differences, our data suggests that activation of DRAIC expression in prostate cancer and gliomas could significantly improve outcomes in these patient populations. In addition, drugs that activate AMPK (like metformin and AICAR) or inhibit mTORC1 (like rapamycin) should be explored for the therapy of GBMs and other tumors with low (or undetectable) levels of DRAIC.

MATERIALS AND METHODS

Cell culture, transfection and microscopy

LNCaP, PC3M, DU145 and U373 cells were maintained in RPMI medium containing 10% fetal bovine serum (FBS), 1% penicillin/streptomycin, 1 mmol/l sodium pyruvate and 10 mmol/l HEPES buffer. HeLa, A172 and U251 and immortalized astrocyte cells were grown in high-glucose DMEM supplemented with 10% FBS and 1% penicillin/streptomycin. U87 cells were cultured in MEM medium with 10% FBS, 1% penicillin/streptomycin, 1 mmol/l sodium pyruvate, 10 ml of 7.5% sodium bicarbonate and 5 ml of 100× nonessential amino acids. Cell culture reagents were obtained from Thermo Fisher Scientific (USA). Glioma stem cells and immortalized astrocytes were cultured according to the previously published protocols (Xie et al., 2020). A172, U87, U251 and U373 cell lines were kind gifts from Dr Roger Abounader (University of Virginia) (Zhang et al., 2017). LNCaP, PC3M, DU145 and HeLa cell lines were procured from ATCC and maintained in humidified incubator at 37°C in the presence of 5% CO_2. All the cell lines were authenticated by short tandem repeats analysis at 15 genomic loci and the amelogenin gene (Biosynthesis). Stable cell lines expressing full-length DRAIC (see below) was generated in PC3M, A172, U87, U373, U251 and HeLa cells. 1 µg of EGFP-LC3B plasmid was transfected with Lipofectamine 3000 into U373 and U251 cells overexpressing either EV or DRAIC. After 48 h of post transfection, cells were imaged with 63× objective using the Zeiss Fluorescence microscope.

Journal of Cell Science (2021) 134, jcs259306. doi:10.1242/jcs.259306

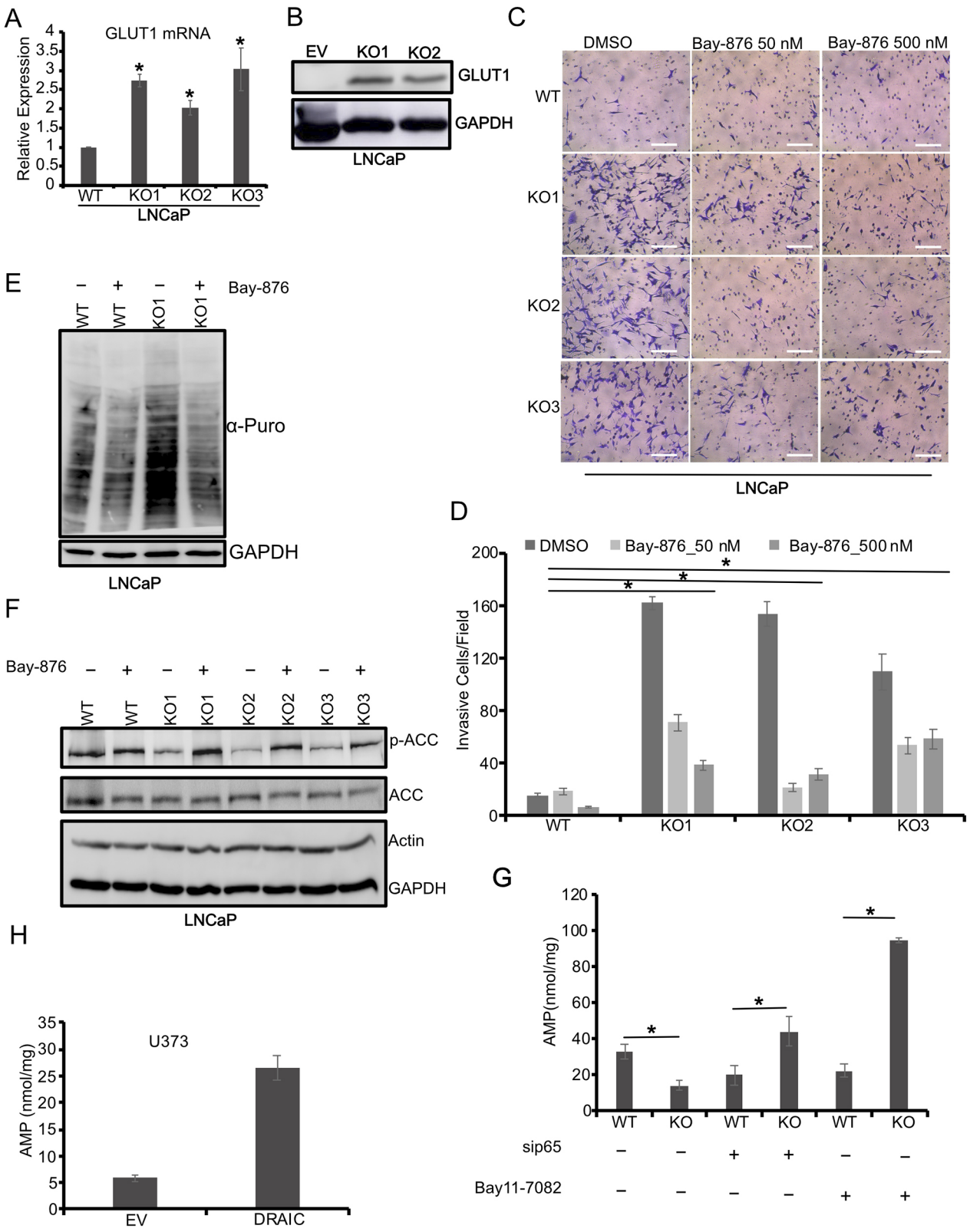

Fig. 7. See next page for legend.

Time-lapse video microscopy

The bright field time-lapse video microscopy was performed to monitor the cell migration with Zeiss Observer Z1 wide-field microscope. The live-cell movement was captured every 10 min for a duration of 24 h using the Zeiss software. The cells were maintained at 37°C in the presence of 5% CO_2.

Plasmids and reagents

The plasmids pcDNA3-Flag-LKB1 (Addgene #8591), pEBG-AMPKα1(1-312) (Addgene #27632) IKK2 K44M (Addgene #1104), pEGFP-LC3 (Addgene #24920) were procured from Addgene. Antibodies against IKKα (#ab109749), IKKβ (#ab32135), Ribosomal S6 (#ab40820), STAT1

Journal of Cell Science (2021) 134, jcs259306. doi:10.1242/jcs.259306

Fig. 7. Induction of protein translation, invasion and AMP target phosphorylation in DRAIC KO cells is reversed with GLUT1 inhibitor. (A) GLUT1 mRNA expression in DRAIC KO LNCaP cells were measured by qRT-PCR. (B) EV and DRAIC KO clones were subjected to immunoblotting with GLUT1 antibody. (C,D) WT and DRAIC KO clones were treated with the GLUT1 inhibitor Bay-876 for 24 h and a Boyden chamber Matrigel invasion assay was carried out. The invasive cells were strained with Crystal Violet and images were captured under a microscope. 8 random fields were captured and quantified. (E) DRAIC KO cells were treated with GLUT1 inhibitor, Bay-876 for 24 h followed by pulse labeling with puromycin and immunoblotting with antibody against puromycin. (F) WT and DRAIC KO clones were treated with Bay-876 for 24 h and immunoblotted with antibodies against phospho-ACC S79, total ACC and internal loading control GAPDH. (G) 2×10^7 cells were lysed with AMP lysis buffer and AMP concentration was measured using BioVision kit. (H) AMP concentration in EV and DRAIC-overexpressing U373 cells according to manufacturer's protocol. Scale bars: 20 µm. Data are presented as mean±s.d. from two independent experiments, each with three technical replicates. *P<0.05 (one-way ANOVA).

(#ab109320) were purchased from Abcam. Antibodies against phosphor-AMPKα (T172) (#2531), AMPKα (#5831), phosphor-mTOR (S2448) (#2971), mTOR (#2972), LC3B (#3868), phosphor-ULK1 (S757) (Cell Signaling, #14202), ULK1 (Cell Signaling, #8054), Phospho Raptor (S792) (#2083), Raptor (#2280), LKB1 (#3050), phospho p70 S6K (T389) (#9234), p70-S6K (#2708), phospho S6 (S235/236), phospho Beclin-1 (S15) (#84996), Beclin-1 (#3495), phospho FoxO3a(S413) (#8174), p62 (#23214), phospho Acetyl-CoA Carboxylase Ser79 (#3661), Acetyl-CoA-Carboxylase (#3676) were purchased from Cell Signaling Technology. Antibody against Raptor (#A300-553A) antibody was purchased from Bethyl Laboratories. Antibodies against α-tubulin (#sc-5286), β-actin (#sc-47778), HSP90 (#sc-13119), GAPDH (#sc-47724) were purchased from Santa Cruz Biotechnology. Puromycin antibody (#MABE343) was purchased from Sigma-Millipore. Anti-GLUT1 antibody was obtained from Proteintech (#21829-1-AP). The shRNA oligonucleotide against DRAIC [shGL2 sense, 5′-TTTGTACGCGGAATACTTCGAAATGC-TTCCTGTCACATTTCGAAGTATTCCGCGTACTTTTTTG-3′; shGL2 antisense: 5′-AATTCAAAAAAGTACGCGGAATACTTCGAAATGTG-ACAGGAAGCATTTCGAAGTATTCCGCGTA-3′; shDRAIC 1 sense, 5′-TTTGCAACTGAAACAACATCTGGAGCTTCCTGTCACTCCAGA-TGTTGTTTCAGTTGCTTTTTTG-3′; shDRAIC 1 antisense, 5′-AATT-CAAAAAAGCAACTGAAACAACATCTGGAGTGACAGGAAGCTCC-AGATGTTGTTTCAGTTG-3′, shDRAIC 2 sense, 5′-TTTGAAACC-TGGGTTTCGACTTGTGCTTCCTGTCACACAAGTCGAAACCCAGG-TTTCTTTTTTG-3′; shDRAIC 2 antisense, 5′-AATTCAAAAAAG-AAACCTGGGTTTCGACTTGTGTGACAGGAAGCACAAGTCGAAA-CCCAGGTTT-3′] were annealed and cloned into pLSP lentivirus vector (a kind gift from Dr Hideo Iba, The University of Tokyo, Tokyo, Japan). Bay11-7082 (#S2913), Bay-876 (#S8452), 5-aminoimidazole-4 carbox-amide-1-β-D-ribofuranoside (AICAR; #S1802), metformin (#S1950), rapamycin (#S1039) and bafilomycin A1 (#S1413) were purchased from Selleckchem. Noble agar (#S5431) was purchased from Sigma.

Electrophoresis and immunoblot analysis

The cells on Petri dishes were washed twice with cold phosphate-buffered saline (pH 7.4) and lysed with lysis buffer [50 mM Tris-HCl pH 8.0, NaCl, 10 mM NaF, 1 mM EDTA, 0.5% NP-40, 1 mM PMSF, 1 mM DTT, 0.5% sodium deoxycholate, Halt protease inhibitor cocktail (Fisher Scientific, #78429) and phosphatase inhibitor tablet (Sigma, #4906845001)]. The lysates were centrifuged at 15,100 ***g*** for 20 min at 4°C and the supernatant was boiled with 1× Laemmli sample buffer and the different amounts of proteins were separated on 10–12% SDS-PAGE gels and immunoblotted with antibodies against phosphor-mTOR S2448 (1:1000), mTOR (1:1000), phosphor-S6K T389 (1:1000), S6K (1:2000), α-tubulin (1:5000), phospho-S6 S235/236 (1:2000), S6 (1:4000), actin (1:5000), puromycin (1:5000), phosphor-AMPK T172 (1:1000), AMPK (1:2000), phosphor-Raptor S792 (1:1000), Raptor (1:2000), phosphor-ULK1 S555 (1:1000), ULK1 (1:2000), GAPDH (1:5000), GLUT1 (1:1000), phosphor-FoxO3a S413 (1:1000), LC3B (1:1000), p62 (1:2000), HSP90 (1:5000), p-acetyl-CoA-carboxylase (1:1000) and acetyl-CoA-Carboxylase (1:1000).

Colony formation, cell proliferation and invasion assay

U87 and A172 cells overexpressing either EV or DRAIC were used for colony formation assay. Briefly, 1000 cells from each condition were plated in each well of six-well plates and incubated at 37°C with 5% CO_2 incubator for around 2 weeks and colonies were stained with 0.05% Crystal Violet

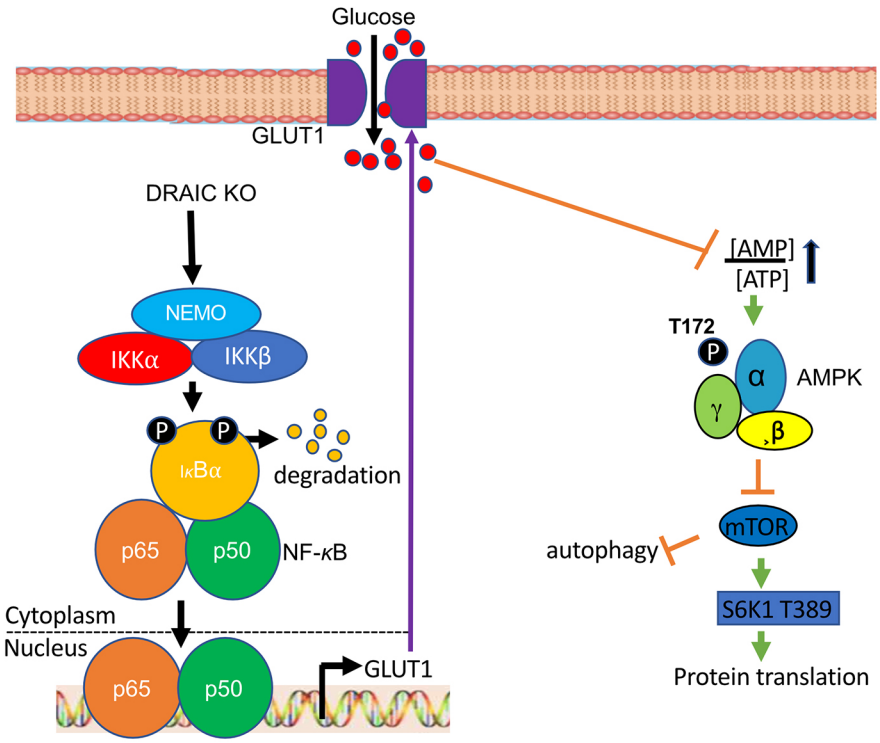

Fig. 8. Model of the pathway by which DRAIC regulates translation, autophagy, migration and invasion and thus acts as a tumor suppressor. Decrease of DRAIC increases expression of the NF-κB target gene GLUT1, which increases glucose uptake, thus decreasing the AMP/ATP ratio and inhibiting AMPK, which stimulates mTOR. See Discussion for further details.

containing 1% formaldehyde and gently rinsed with water. The plates were dried and imaged with a scanner. The MTT assay was performed as described previously (Saha et al., 2020). Briefly, 5×10^4 cells stably transfected with EV and DRAIC were seeded in 24-well plates and an MTT assay was performed at different days. The Matrigel-containing Boyden chamber invasion assay was carried out as described previously (Saha et al., 2020). EV and DRAIC KO cells were transfected with constitutive active AMPK or pre-treated the cells with rapamycin and AMPK activator AICAR for 24 h. The cells were trypsinized, and a total of 1×10^5 cells were added in serum-free medium in the top of the chamber and full growth medium containing 10% FBS was added to the bottom of the chamber as a chemoattractant, and the chamber incubated at 37°C in the presence of 5% CO_2 for 24 h. After 16–24 h, the invaded cells on the bottom surface of the membrane were gently washed with 1× PBS and fixed with 100% methanol for 5 min followed by 0.5% Crystal Violet staining at room temperature for 15 min. The non-invading cells from the top surface of the chamber were removed by cotton swab. Ten random fields were captured under the microscope and the invaded cell numbers were quantified using ImageJ software.

RNA isolation and cDNA synthesis and quantitative PCR

Total RNA was isolated from cells using TRIzol (Thermo Fisher Scientific, #15596018) according to the manufacturer's protocol. 1 µg of total RNA was treated with DNase I (#M0303) and reverse transcribed using SuperScript III First-Strand cDNA synthesis kit (Thermo Fisher Scientific, #18080051). The resulting cDNAs were quantified using the real time PCR (StepOne Plus, Thermo Fisher Scientific) to check the expression of autophagy-responsive gene expression with the primer set (Table S1). The qPCR fold change was calculated using the $\Delta\Delta C_t$ method after normalizing with loading control actin RNA or GAPDH (Table S1).

Anchorage-independent growth assay

Soft agar colony formation assay was performed as described previously (Saha et al., 2020). Briefly, the bottom layer of soft agar was prepared by mixing equal volume of 1% sterile noble agar, which was maintained at 40°C (Sigma-Aldrich, catalog no. A5431) and 2× growth medium and kept at room temperature for 30 min to solidify. For the top layer, 1×10^4 cells were resuspended with equal volume of 2× growth medium and 0.6% soft agar, which was also maintained at 40°C and added dropwise on the bottom agar layer. The plates were allowed to solidify for an additional 30 min at room temperature. The plates were then kept in a humidified chamber at 37°C in the presence of 5% CO_2 for an additional 3–4 weeks. The visible colonies were captured using 4× bright field objective. Ten random microscopic fields were used for quantification. ImageJ software was used for calculating the colony number and size.

Measurement of AMP concentration

AMP concentration was measured according to the manufacturer's protocol (BioVision #K229). Briefly, 2×10^7 cells from WT and DRAIC KO LNCaP cells were harvested either treated with Bay11-7082 or subjected to p65 knockdown with siRNA (Saha et al., 2020). The cells pellet was washed with 1× PBS, pH 7.4 and lysed with AMP assay buffer and centrifuged at 10,000 ***g*** for 10 min. The protein concentration was measured, and equal amount of protein was used for the assay. The absorbance of the colored product was measured at 570 nm. The AMP concentration of the WT and DRAIC KO cells were measured from the AMP standard curve and expressed as nmol/mg.

Mouse xenograft

The effect of DRAIC overexpression on tumor growth *in vivo* was validated by intracranial mouse xenograft model. Six-week-old athymic nude male mice were procured from The Jackson Laboratory and mice experiments were carried out according to the University of Virginia institutional guidelines. A total of 2×10^5 U87 cells stably transfected with either EV (n=9) or DRAIC long noncoding RNA (n=9) were stereotactically implanted into the striata of immunodeficient mice. After 3 weeks of injection, mice were subjected to MRI imaging. MRI was used to monitor intracranial tumor growth and measurement for the tumor volume *in vivo*. Prior to imaging, gadopentetate dimeglumine was injected intraperipherally to increase the signal intensity of tumor relative to healthy brain on MRI. T1-weighted serial coronal images of each brain was acquired at 1 mm intervals with a 2.5 mm×2.5 mm field and a 256×256 pixel resolution. Acquired DICOM images was converted into JPEG format and for analysis of tumor volumes using ImageJ software (NIH, USA).

DRAIC exon 2-4 knockout by CRISPR/Cas9

DRAIC KO LNCaP cells were prepared by CRISPR/Cas9 system according to the method in our previous publication (Saha et al., 2020). Briefly, sgRNAs targeting DRAIC exon 2 and 4 were designed using http://crispr.mit.edu/. The sgRNAs were annealed and ligated with quick ligation mixture into px333 vector, which was digested separately with Bbs1 and Bsa1 restriction enzymes, respectively. The LNCaP cells were transfected with px333 plasmid containing both the sgRNAs targeting DRAIC exon 2 and exon 4 and selected with the 500 µg/ml antibiotic marker G418. The selected heterogenous resistant population were plated into a 96-well plate for single-cell expansion. The genomic DNA was isolated from each single clone using the quick genomic DNA isolation kit and DRAIC genomic deletion was confirmed both by PCR and Sanger sequencing.

Statistical analysis

All data are expressed as mean±s.d. from indicated numbers of measurements. The significance was calculated by Student's *t*-test (paired test, two sided) when comparing with two samples. One-way analysis of variance (ANOVA) followed by Bonferroni test was carried out to determine the statistical significance while comparing with multiple samples. The differences are called statistically significant if the *P*-value is <0.05.

Acknowledgements

We acknowledge the MAPS core facility at University of Virginia for helping with the animal experiment. We thank Dr Hui Li's group, University of Virginia for providing cDNA samples from glioma stem cells and Dr Manikarna Dinda for preparing the graphical summary and for reading the manuscript.

Competing interests

The authors declare no competing or financial interests.

Author contributions

Conceptualization: S.S., A.D.; Methodology: S.S., Y.Z.; Validation: S.S.; Formal analysis: S.S.; Investigation: S.S., A.D.; Resources: A.D.; Data curation: S.S., Y.Z., B.W.; Writing - original draft: S.S.; Writing - review & editing: S.S., B.W., R.A., A.D.; Visualization: S.S., A.D.; Supervision: R.A., A.D.; Funding acquisition: A.D.

Funding

This work was supported by the National Institutes of Health (R01 AR067712 and R01 CA060499 to A.D., and P30 CA44579 to S.S.). Deposited in PMC for release after 12 months.

Peer review history

The peer review history is available online at https://journals.biologists.com/jcs/article-lookup/doi/10.1242/jcs.259306.

References

Adamson, C., Kanu, O. O., Mehta, A. I., Di, C., Lin, N., Mattox, A. K. and Bigner, D. D. (2009). Glioblastoma multiforme: a review of where we have been and where we are going. *Expert Opin Investig. Drugs* **18**, 1061-1083. doi:10.1517/13543780903052764

Alers, S., Löffler, A. S., Wesselborg, S. and Stork, B. (2012). Role of AMPK-mTOR-Ulk1/2 in the regulation of autophagy: cross talk, shortcuts, and feedbacks. *Mol Cell. Biol.* **32**, 2-11. doi:10.1128/MCB.06159-11

Anjum, K., Shagufta, B. I., Abbas, S. Q., Patel, S., Khan, I., Shah, S. A. A., Akhter, N. and Hassan, S. S. U. (2017). Current status and future therapeutic perspectives of glioblastoma multiforme (GBM) therapy: a review. *Biomed. Pharmacother.* **92**, 681-689. doi:10.1016/j.biopha.2017.05.125

Bhan, A. and Mandal, S. S. (2014). Long noncoding RNAs: emerging stars in gene regulation, epigenetics and human disease. *ChemMedChem* **9**, 1932-1956. doi:10.1002/cmdc.201300534

Chen, J.-F., Wu, P., Xia, R., Yang, J., Huo, X.-Y., Gu, D.-Y., Tang, C.-J., De, W. and Yang, F. (2018). STAT3-induced lncRNA HAGLROS overexpression contributes to the malignant progression of gastric cancer cells via mTOR signal-mediated inhibition of autophagy. *Mol. Cancer* **17**, 6. doi:10.1186/s12943-017-0756-y

Chiang, G. G. and Abraham, R. T. (2005). Phosphorylation of mammalian target of rapamycin (mTOR) at Ser-2448 is mediated by p70S6 kinase. *J. Biol. Chem.* **280**, 25485-25490. doi:10.1074/jbc.M501707200

Chittaranjan, S., Bortnik, S., Dragowska, W. H., Xu, J., Abeysundara, N., Leung, A., Go, N. E., DeVorkin, L., Weppler, S. A., Gelmon, K. et al. (2014). Autophagy inhibition augments the anticancer effects of epirubicin treatment in anthracycline-sensitive and-resistant triple-negative breast cancer. *Clin. Cancer Res.* **20**, 3159-3173. doi:10.1158/1078-0432.CCR-13-2060

Cohen-Kaplan, V., Livneh, I., Avni, N., Fabre, B., Ziv, T., Kwon, Y. T. and Ciechanover, A. (2016). p62-and ubiquitin-dependent stress-induced autophagy of the mammalian 26S proteasome. *Proc. Natl Acad. Sci. USA* **113**, E7490-E7499. doi:10.1073/pnas.1615455113

Dan, H. C., Cooper, M. J., Cogswell, P. C., Duncan, J. A., Ting, J. P.-Y. and Baldwin, A. S. (2008). Akt-dependent regulation of NF-κB is controlled by mTOR and Raptor in association with IKK. *Genes Dev.* **22**, 1490-1500. doi:10.1101/gad.1662308

Demuth, T. and Berens, M. E. (2004). Molecular mechanisms of glioma cell migration and invasion. *J. Neurooncol.* **70**, 217-228. doi:10.1007/s11060-004-2751-6

Du, Y., Wang, L., Chen, S., Liu, Y. and Zhao, Y. (2018). lncRNA DLEU1 contributes to tumorigenesis and development of endometrial carcinoma by targeting mTOR. *Mol. Carcinog.* **57**, 1191-1200. doi:10.1002/mc.22835

Easton, J. B. and Houghton, P. J. (2006). mTOR and cancer therapy. *Oncogene* **25**, 6436-6446. doi:10.1038/sj.onc.1209886

Egan, D., Kim, J., Shaw, R. J. and Guan, K.-L. (2011a). The autophagy initiating kinase ULK1 is regulated via opposing phosphorylation by AMPK and mTOR. *Autophagy* **7**, 643-644. doi:10.4161/auto.7.6.15123

Egan, D. F., Shackelford, D. B., Mihaylova, M. M., Gelino, S., Kohnz, R. A., Mair, W., Vasquez, D. S., Joshi, A., Gwinn, D. M., Taylor, R. et al. (2011b). Phosphorylation of ULK1 (hATG1) by AMP-activated protein kinase connects energy sensing to mitophagy. *Science* **331**, 456-461. doi:10.1126/science.1196371

Guertin, D. A. and Sabatini, D. M. (2007). Defining the role of mTOR in cancer. *Cancer Cell* **12**, 9-22. doi:10.1016/j.ccr.2007.05.008

Gupta, R. A., Shah, N., Wang, K. C., Kim, J., Horlings, H. M., Wong, D. J., Tsai, M.-C., Hung, T., Argani, P., Rinn, J. L. et al. (2010). Long non-coding RNA HOTAIR reprograms chromatin state to promote cancer metastasis. *Nature* **464**, 1071-1076. doi:10.1038/nature08975

Gutschner, T. and Diederichs, S. (2012). The hallmarks of cancer: a long non-coding RNA point of view. *RNA Biol.* **9**, 703-719. doi:10.4161/rna.20481

Gwinn, D. M., Shackelford, D. B., Egan, D. F., Mihaylova, M. M., Mery, A., Vasquez, D. S., Turk, B. E. and Shaw, R. J. (2008). AMPK phosphorylation of raptor mediates a metabolic checkpoint. *Mol. Cell* **30**, 214-226. doi:10.1016/j.molcel.2008.03.003

Hajjari, M. and Salavaty, A. (2015). HOTAIR: an oncogenic long non-coding RNA in different cancers. *Cancer Biol. Med.* **12**, 1.

Hardie, D. G. and Ashford, M. L. J. (2014). AMPK: regulating energy balance at the cellular and whole body levels. *Physiology* **29**, 99-107. doi:10.1152/physiol.00050.2013

Holz, M. K., Ballif, B. A., Gygi, S. P. and Blenis, J. (2005). mTOR and S6K1 mediate assembly of the translation preinitiation complex through dynamic protein interchange and ordered phosphorylation events. *Cell* **123**, 569-580. doi:10.1016/j.cell.2005.10.024

Hung, T. and Chang, H. Y. (2010). Long noncoding RNA in genome regulation: prospects and mechanisms. *RNA Biol.* **7**, 582-585. doi:10.4161/rna.7.5.13216

Inoki, K., Zhu, T. and Guan, K.-L. (2003). TSC2 mediates cellular energy response to control cell growth and survival. *Cell* **115**, 577-590. doi:10.1016/S0092-8674(03)00929-2

Jiang, J., Zhang, L., Chen, H., Lei, Y., Zhang, T., Wang, Y., Jin, P., Lan, J., Zhou, L., Huang, Z. et al. (2020). Regorafenib induces lethal autophagy arrest by stabilizing PSAT1 in glioblastoma. *Autophagy* **16**, 106-122. doi:10.1080/15548627.2019.1598752

Jung, C. H., Ro, S.-H., Cao, J., Otto, N. M. and Kim, D.-H. (2010). mTOR regulation of autophagy. *FEBS Lett.* **584**, 1287-1295. doi:10.1016/j.febslet.2010.01.017

Kim, Y. C. and Guan, K.-L. (2015). mTOR: a pharmacologic target for autophagy regulation. *J. Clin. Investig.* **125**, 25-32. doi:10.1172/JCI73939

Kim, J., Kundu, M., Viollet, B. and Guan, K.-L. (2011). AMPK and mTOR regulate autophagy through direct phosphorylation of Ulk1. *Nat. Cell Biol.* **13**, 132-141. doi:10.1038/ncb2152

Levy, J. M. M., Towers, C. G. and Thorburn, A. (2017). Targeting autophagy in cancer. *Nat. Rev. Cancer* **17**, 528-542. doi:10.1038/nrc.2017.53

Li, Z., Yang, Z., Passaniti, A., Lapidus, R. G., Liu, X., Cullen, K. J. and Dan, H. C. (2016). A positive feedback loop involving EGFR/Akt/mTORC1 and IKK/NF-κB regulates head and neck squamous cell carcinoma proliferation. *Oncotarget* **7**, 31892. doi:10.18632/oncotarget.7441

Mair, D. B., Ames, H. M. and Li, R. (2018). Mechanisms of invasion and motility of high-grade gliomas in the brain. *Mol. Biol Cell* **29**, 2509-2515. doi:10.1091/mbc.E18-02-0123

Malakar, P., Shilo, A., Mogilevsky, A., Stein, I., Pikarsky, E., Nevo, Y., Benyamini, H., Elgavish, S., Zong, X., Prasanth, K. V. et al. (2017). Long noncoding RNA MALAT1 promotes hepatocellular carcinoma development by SRSF1 upregulation and mTOR activation. *Cancer Res.* **77**, 1155-1167. doi:10.1158/0008-5472.CAN-16-1508

Malek, E., Jagannathan, S. and Driscoll, J. J. (2014). Correlation of long non-coding RNA expression with metastasis, drug resistance and clinical outcome in cancer. *Oncotarget* **5**, 8027. doi:10.18632/oncotarget.2469

Mammucari, C., Milan, G., Romanello, V., Masiero, E., Rudolf, R., Del Piccolo, P., Burden, S. J., Di Lisi, R., Sandri, C. and Zhao, J. (2007). FoxO3 controls autophagy in skeletal muscle in vivo. *Cell Metab.* **6**, 458-471. doi:10.1016/j.cmet.2007.11.001

Nakamura, S. and Yoshimori, T. (2017). New insights into autophagosome–lysosome fusion. *J. Cell Sci.* **130**, 1209-1216. doi:10.1242/jcs.196352

Pópulo, H., Lopes, J. M. and Soares, P. (2012). The mTOR signalling pathway in human cancer. *Int. J. Mol. Sci.* **13**, 1886-1918. doi:10.3390/ijms13021886

Raizer, J. J., Abrey, L. E., Lassman, A. B., Chang, S. M., Lamborn, K. R., Kuhn, J. G., Yung, W. K. A., Gilbert, M. R., Aldape, K. A., Wen, P. Y. et al. (2010). A phase II trial of erlotinib in patients with recurrent malignant gliomas and nonprogressive glioblastoma multiforme postradiation therapy. *Neuro Oncol.* **12**, 95-103. doi:10.1093/neuonc/nop015

Ransohoff, J. D., Wei, Y. and Khavari, P. A. (2018). The functions and unique features of long intergenic non-coding RNA. *Nat. Rev. Mol. Cell Biol.* **19**, 143. doi:10.1038/nrm.2017.104

Saha, S., Kiran, M., Kuscu, C., Chatrath, A., Wotton, D., Mayo, M. W. and Dutta, A. (2020). Long noncoding RNA DRAIC inhibits prostate cancer progression by interacting with IKK to inhibit NF-κB activation. *Cancer Res.* **80**, 950-963. doi:10.1158/0008-5472.CAN-19-3460

Sakurai, K., Reon, B. J., Anaya, J. and Dutta, A. (2015). The lncRNA DRAIC/PCAT29 locus constitutes a tumor-suppressive nexus. *Mol. Cancer Res.* **13**, 828-838. doi:10.1158/1541-7786.MCR-15-0016-T

Sanchez, A. M. J., Csibi, A., Raibon, A., Cornille, K., Gay, S., Bernardi, H. and Candau, R. (2012). AMPK promotes skeletal muscle autophagy through activation of forkhead FoxO3a and interaction with Ulk1. *J. Cell. Biochem.* **113**, 695-710. doi:10.1002/jcb.23399

Sanchez Calle, A., Kawamura, Y., Yamamoto, Y., Takeshita, F. and Ochiya, T. (2018). Emerging roles of long non–coding RNA in cancer. *Cancer Sci.* **109**, 2093-2100. doi:10.1111/cas.13642

Sarbassov, D. D., Ali, S. M. and Sabatini, D. M. (2005). Growing roles for the mTOR pathway. *Curr. Opin. Cell Biol.* **17**, 596-603. doi:10.1016/j.ceb.2005.09.009

Shaw, R. J. (2009). LKB1 and AMP-activated protein kinase control of mTOR signalling and growth. *Acta Physiol.* **196**, 65-80. doi:10.1111/j.1748-1716.2009.01972.x

Statello, L., Guo, C.-J., Chen, L.-L. and Huarte, M. (2021). Gene regulation by long non-coding RNAs and its biological functions. *Nat. Rev. Mol. Cell Biol.* **22**, 96-118. doi:10.1038/s41580-020-00315-9

Sun, M., Gadad, S. S., Kim, D.-S. and Kraus, W. L. (2015). Discovery, annotation, and functional analysis of long noncoding RNAs controlling cell-cycle gene expression and proliferation in breast cancer cells. *Mol. Cell* **59**, 698-711. doi:10.1016/j.molcel.2015.06.023

Taylor, M. A., Das, B. C. and Ray, S. K. (2018). Targeting autophagy for combating chemoresistance and radioresistance in glioblastoma. *Apoptosis* **23**, 563-575. doi:10.1007/s10495-018-1480-9

Tiessen, I., Abildgaard, M. H., Lubas, M., Gylling, H. M., Steinhauer, C., Pietras, E. J., Diederichs, S., Frankel, L. B. and Lund, A. H. (2019). A high-throughput screen identifies the long non-coding RNA DRAIC as a regulator of autophagy. *Oncogene* **38**, 5127-5141. doi:10.1038/s41388-019-0783-9

Urbańska, K., Sokołowska, J., Szmidt, M. and Sysa, P. (2014). Glioblastoma multiforme–an overview. *Contemp. Oncol.* **18**, 307-312. doi:10.5114/wo.2014.40559

Wang, X. and Proud, C. G. (2006). The mTOR pathway in the control of protein synthesis. *Physiology* **21**, 362-369. doi:10.1152/physiol.00024.2006

Wang, X., Liu, R., Qu, X., Yu, H., Chu, H., Zhang, Y., Zhu, W., Wu, X., Gao, H., Tao, B. et al. (2019). α-Ketoglutarate-activated NF-κB signaling promotes compensatory glucose uptake and brain tumor development. *Mol. Cell* **76**, 148-162.e7. doi:10.1016/j.molcel.2019.07.007

Wen, P. Y., Weller, M., Lee, E. Q., Alexander, B. M., Barnholtz-Sloan, J. S., Barthel, F. P., Batchelor, T. T., Bindra, R. S., Chang, S. M., Chiocca, E. A. et al. (2020). Glioblastoma in adults: a Society for Neuro-Oncology (SNO) and European Society of Neuro-Oncology (EANO) consensus review on current management and future directions. *Neuro Oncol.* **22**, 1073-1113. doi:10.1093/neuonc/noaa106

White, E. (2012). Deconvoluting the context-dependent role for autophagy in cancer. *Nat. Rev. Cancer* **12**, 401-410. doi:10.1038/nrc3262

Wu, Z. R., Yan, L., Liu, Y. T., Cao, L., Guo, Y. H., Zhang, Y., Yao, H., Cai, L., Shang, H. B., Rui, W. W. et al. (2018). Inhibition of mTORC1 by lncRNA H19 via disrupting 4E-BP1/Raptor interaction in pituitary tumours. *Nat. Commun.* **9**, 4624. doi:10.1038/s41467-018-06853-3

Xia, Y., Shen, S. and Verma, I. M. (2014). NF-κB, an active player in human cancers. *Cancer Immunol. Res.* **2**, 823-830. doi:10.1158/2326-6066.CIR-14-0112

Xiao, B., Sanders, M. J., Underwood, E., Heath, R., Mayer, F. V., Carmena, D., Jing, C., Walker, P. A., Eccleston, J. F. and Haire, L. F. (2011). Structure of mammalian AMPK and its regulation by ADP. *Nature* **472**, 230-233. doi:10.1038/nature09932

Xie, Z., Janczyk, P. Ł., Zhang, Y., Liu, A., Shi, X., Singh, S., Facemire, L., Kubow, K., Li, Z., Jia, Y. et al. (2020). A cytoskeleton regulator AVIL drives tumorigenesis in glioblastoma. *Nat. Commun.* **11**, 3457. doi:10.1038/s41467-020-17279-1

Xu, J., Ji, J. and Yan, X.-H. (2012). Cross-talk between AMPK and mTOR in regulating energy balance. *Crit. Rev. Food Sci. Nutr.* **52**, 373-381. doi:10.1080/10408398.2010.500245

Xue, J., Zhong, S., Sun, B.-m., Sun, Q.-F., Hu, L.-Y. and Pan, S.-J. (2019). lncTHOR silencing inhibits human glioma cell survival by activating MAGEA6-AMPK signaling. *Cell Death Dis.* **10**, 866. doi:10.1038/s41419-019-2093-0

Yoon, J.-H., Abdelmohsen, K. and Gorospe, M. (2013). Posttranscriptional gene regulation by long noncoding RNA. *J. Mol. Biol.* **425**, 3723-3730. doi:10.1016/j.jmb.2012.11.024

Zhang, Y., Cruickshanks, N., Yuan, F., Wang, B., Pahuski, M., Wulfkuhle, J., Gallagher, I., Koeppel, A. F., Hatef, S. and Papanicolas, C. (2017). Targetable T-type calcium channels drive glioblastoma. *Cancer Res.* **77**, 3479-3490. doi:10.1158/0008-5472.CAN-16-2347

Zhao, D. and Dong, J.-T. (2018). Upregulation of long non-coding RNA DRAIC correlates with adverse features of breast cancer. *Non-Coding RNA* **4**, 39. doi:10.3390/ncrna4040039

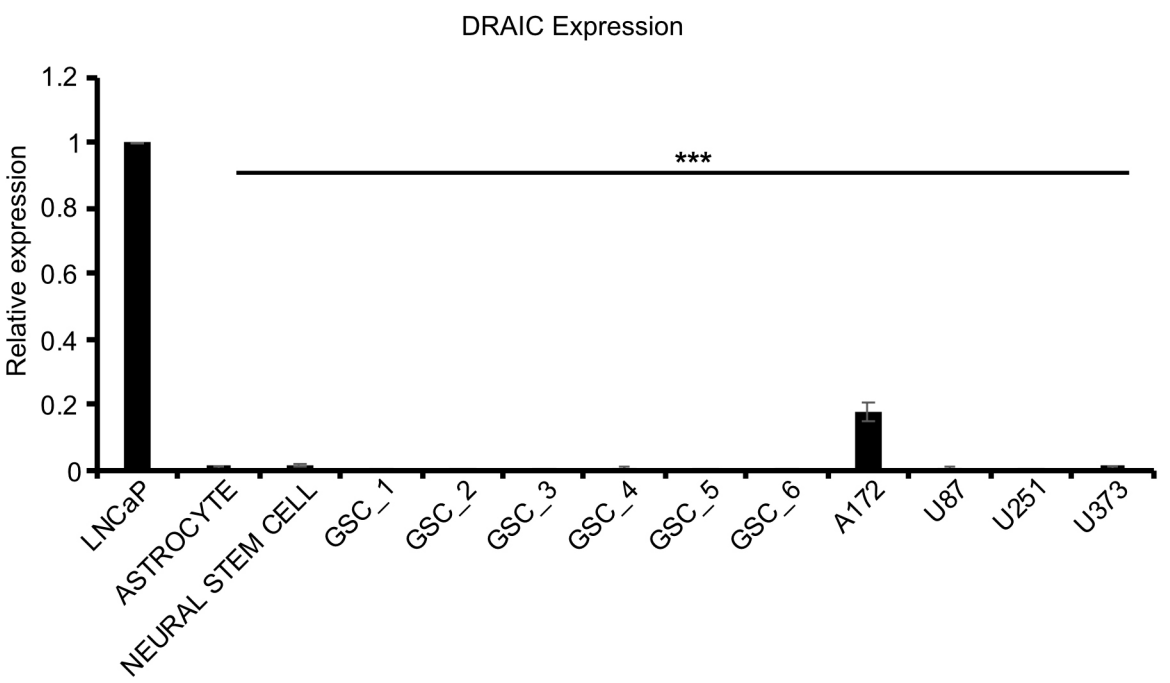

Fig. S1. Endogenous DRAIC expression is low in glioma cell lines: The expression of DRAIC is measured in a panel of glioblastoma cell lines and glioma stem cells derived from patients by RT-qPCR. GAPDH is used as an internal control for RT-qPCR normalization. The DRAIC expression in LNCaP cells is used as 1 for comparison. Data are presented as mean ± SD, *** , $p<0.001$.

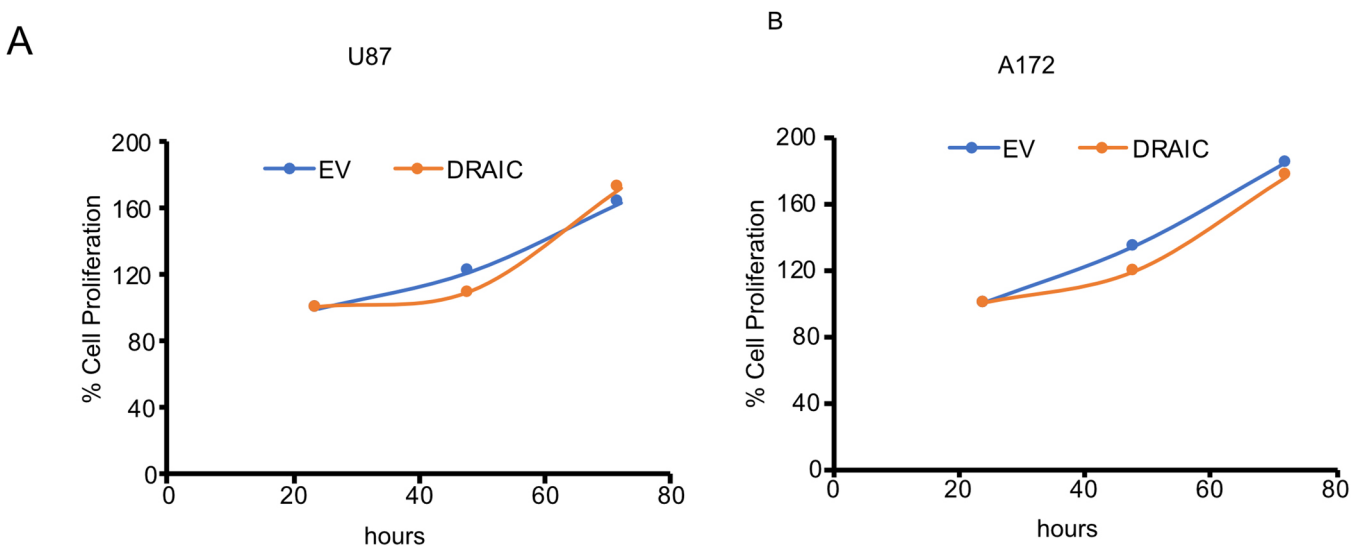

Fig. S2. roliferation of cells ad erent on plastic was unc anged w en DRAIC is overexpressed in glio lastoma cells: A-B) U87 (A) and A172 (B) cells transfected either with EV or DRAIC and MTT assay was performed at different time points.

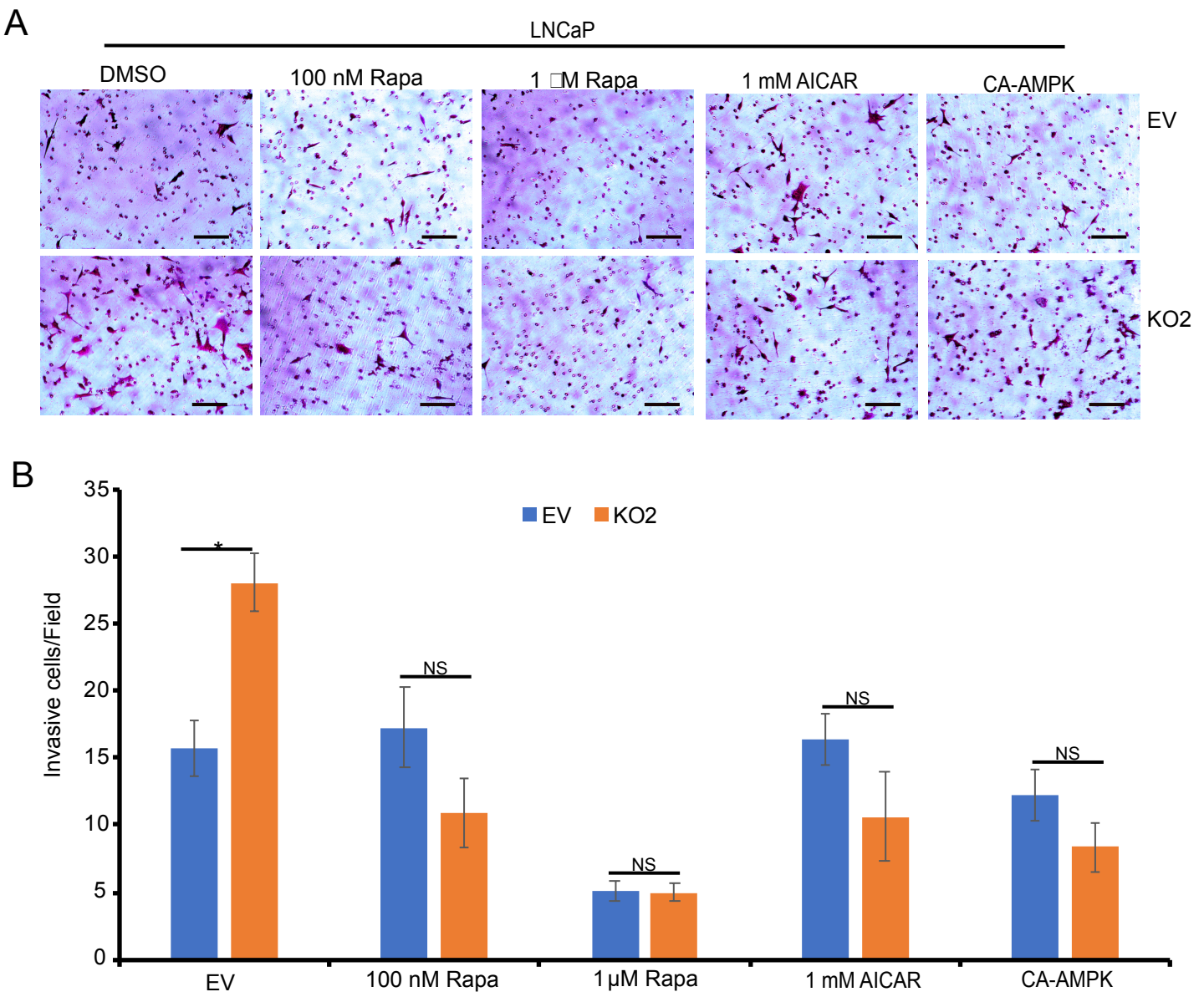

Fig. S3. DRAIC KO induced invasion can be reversed by AMPK activators: A-B) WT and DRAIC KO LNCaP cells were transfected with either EV or constitutive active AMPK or pre-treated cells with 0.1 and 1 μM rapamycin or 1 mM AMPK activator AICAR for 24 hrs and Matrigel Boyden chamber invasion assay was performed (A). The invaded cells were stained with 0.5% crystal violet and imaged with microscope. 10 random fields were selected for counting (**B**). Data are presented as mean ± SD *, $p<0.05$. Scale bar 20 μm

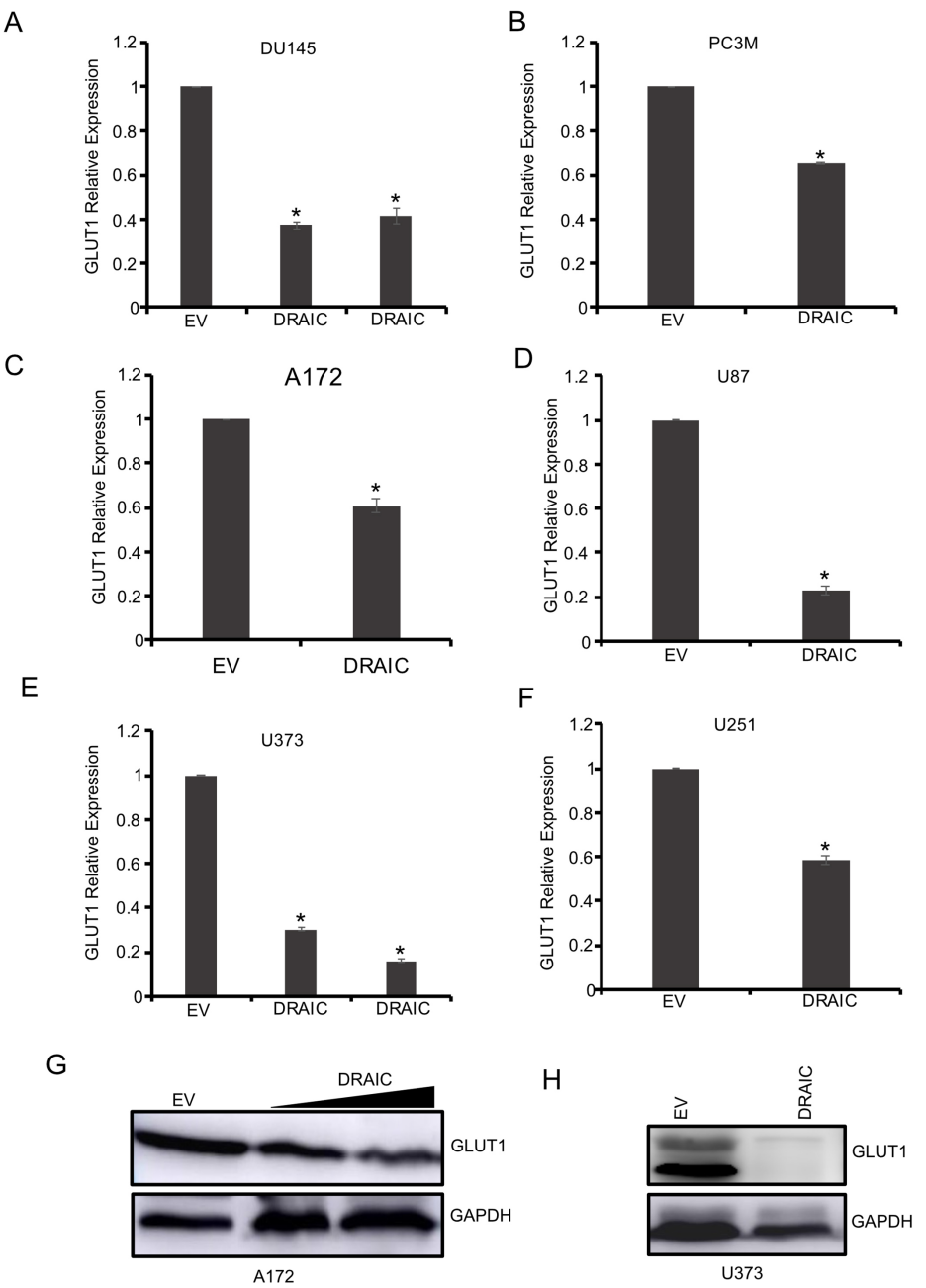

Fig. S4. DRAIC overexpression decreases GLUT1 expression in different cell lines: A-F) GLUT1 mRNA level is measured by RT-qPCR in prostate cancer cell lines DU145 (**A**) and PC3M (**B**) cells and glioblastoma cell lines, A172 (**C**), U87 (**D**), U373 (**E**), U251 (**F**). **G**, **H**) A172 (**G**) and U373 (**H**) cells overexpressing either EV or DRAIC and cell lysates were immunoblotted with GLUT1 antibody. Data are presented as mean ± SD, * , $p<0.05$.

Table S1. Q-RT-PCR primers used in this paper.

Gene	Se uence
p 2	GTGAATTCGCTCGCCGCTCGCTAT
p 2 R	CGTCTCGAGTGCCTGCTGACAACACCTA
LC3B	AGCAGCATCCAACCAAAATC
LC3B R	CTGTGTCCGTTCACCAACAG
GABARAPL1	GCACAATACTGGATGCCGTC
GABARAPL1 R	CCTTCTGCCCCACTTCTCAG
GAPDH	ACTGGCGTCTTCACCACCAT
GAPDH R	GCAGGAGGCATTGCTGATGA
DRAIC 1	AAGGCCTACCTCATTGGGCTC
DRAIC 2	GCTTGTTCTTTTCTGGGTCTCTCC
DRAIC 2R	GGCACTCTACAGTGTGCAGATG
DRAIC 3	CTTGGGAAATTTGAAGTGGAGTACCTG
DRAIC 3R	TTTCATTAATGACACCTGATTTTGGAGGC
DRAIC 4	TGAACTTCAAAGGGCAGAGGGG
DRAIC 4R	TTAACCCGGGTCTTCTGCGC
GLUT1_F	TGGCATCAACGCTGTCTTCT
GLUT1_R	AGCCAATGGTGGCATACACA

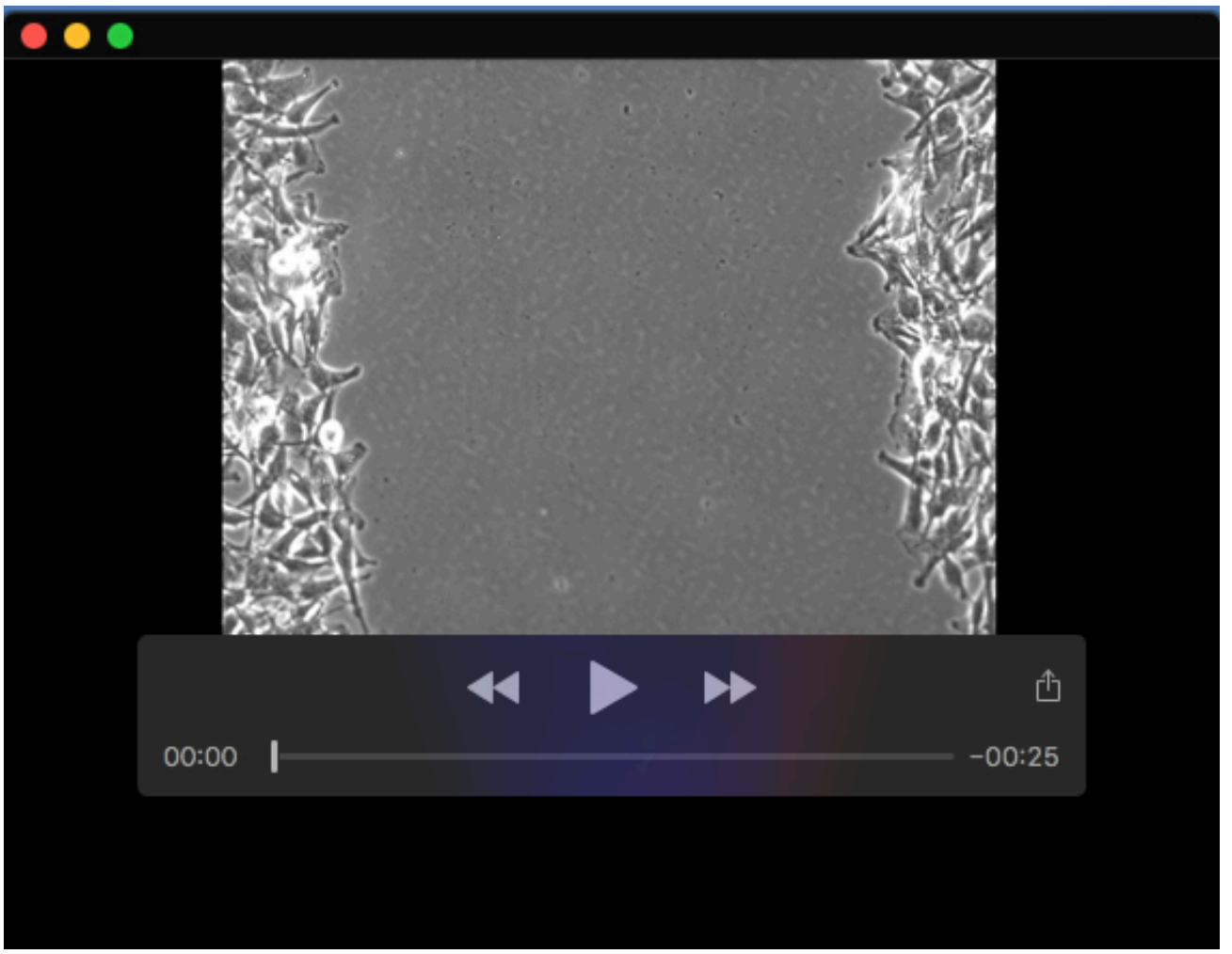

Movie 1. Cell migration was assessed by Time lapse microscopy in A172 cells stably overexpressing EV.

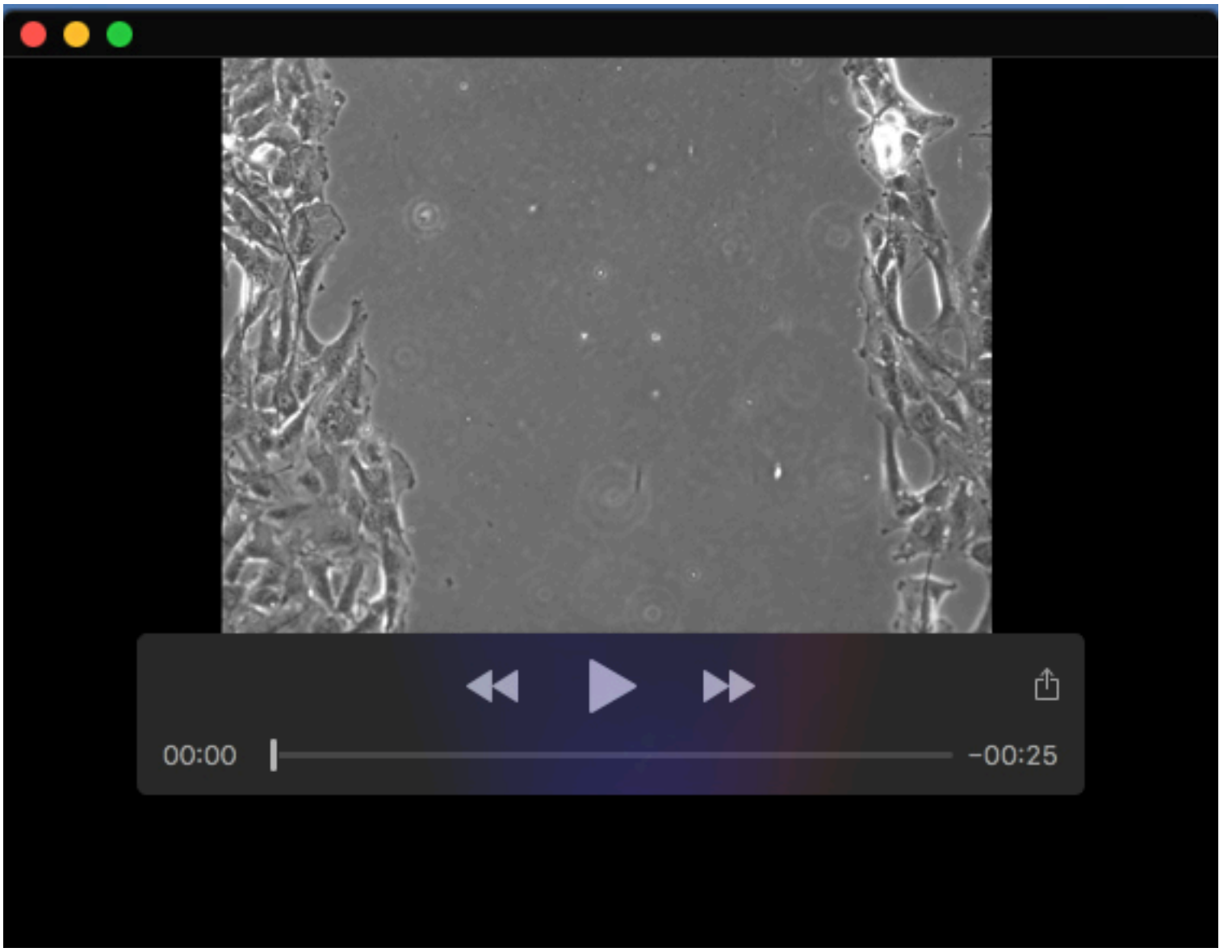

Movie 2. Cell migration was assessed by Time lapse microscopy in A172 cells stably overexpressing full length DRAIC.

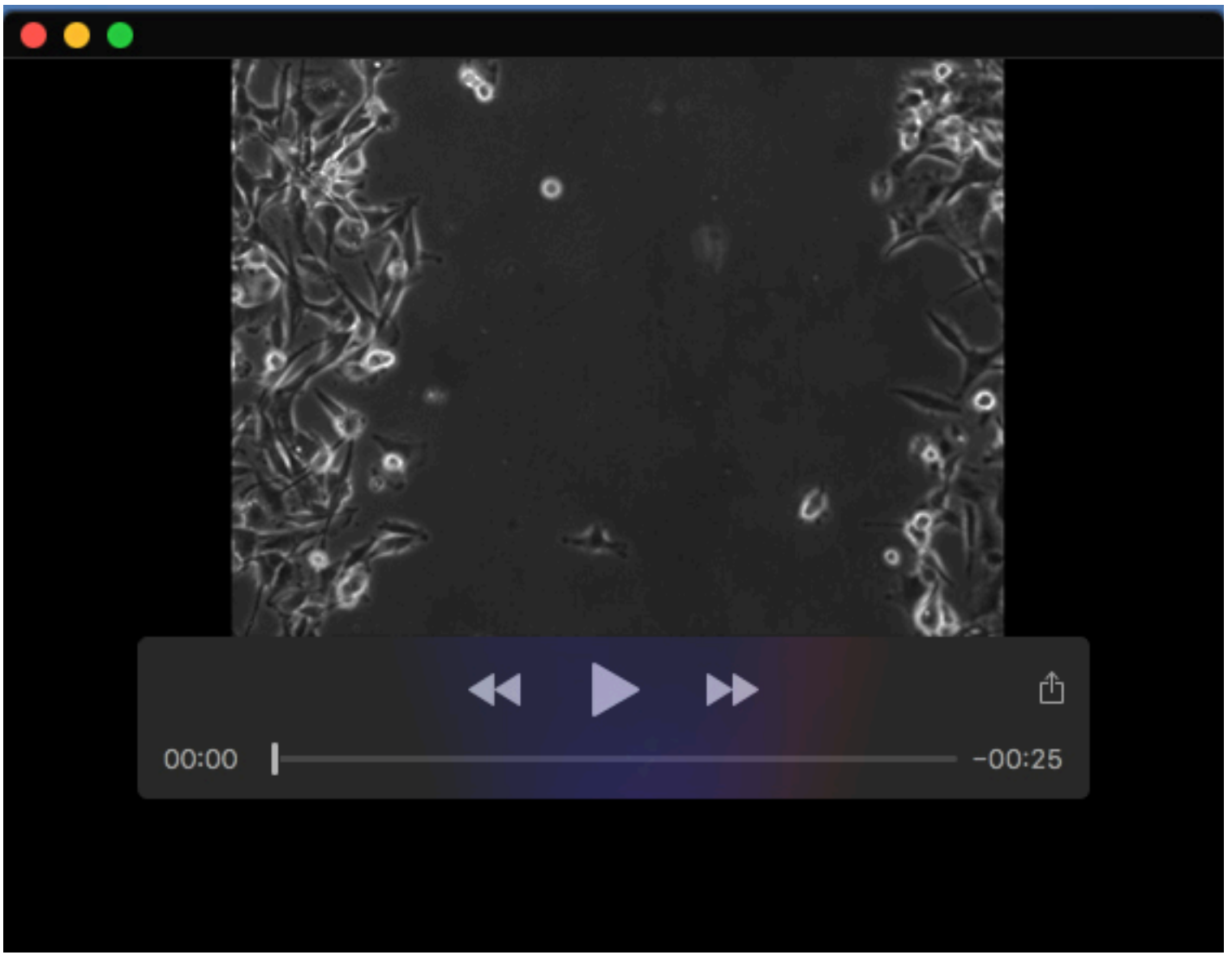

Movie 3. Cell migration was assessed by Time lapse microscopy in U87 cells stably overexpressing EV.

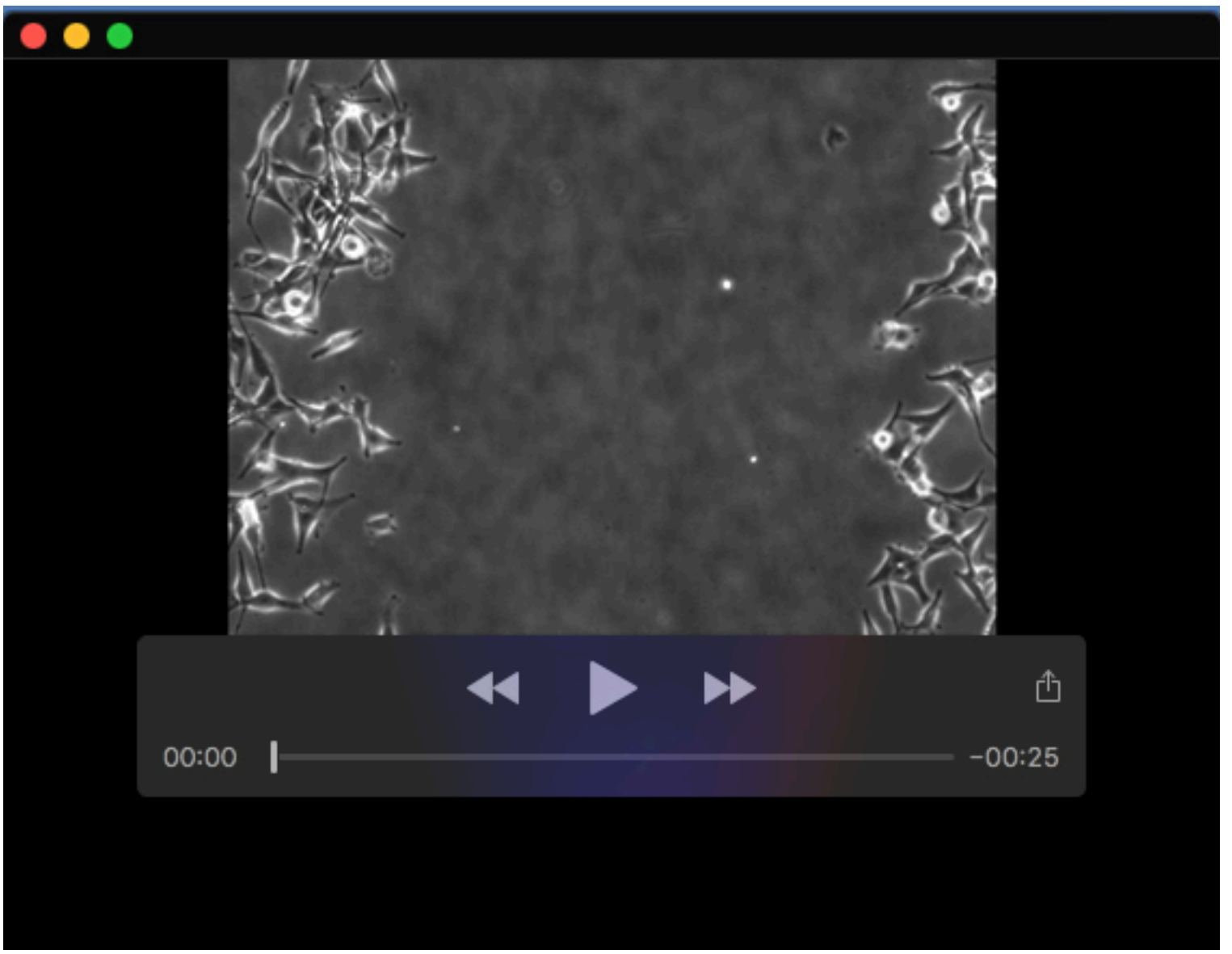

Movie 4. Cell migration was assessed by Time lapse microscopy in U87 cells stably overexpressing full length DRAIC.

Journal of Cell Science • Supplementary information